Fluorescence Polarization Spectroscopy at Combined High-Aperture Excitation and Detection: Application to One-Photon-Excitation Fluorescence Microscopy†

Jacek J. Fisz*

Institute of Physics, Nicolaus Copernicus University, ul. Grudzidzka 5/7, PL 87-100 Toruń, Poland

Received: March 16, 2007; In Final Form: June 26, 2007

A problem of the one-photon-excitation fluorescence polarization spectroscopy of macroscopically isotropic media, in the case of combined high-aperture excitation and detection, is considered and described in a spherical representation. The case of inhomogeneous intensity distribution in the cross-section of the parallel beam of exciting light, which is converted by an objective lens into inhomogeneous radial distribution of the intensity of the focused exciting light, is also taken into account. The obtained formalism is adapted to the description of confocal fluorescence polarization microscopy. It is shown that the total and magic-angle-detected fluorescence decays do not solely represent the kinetic evolution of the excited-state because of the contribution of the dynamic evolution of photoselected fluorophores. The time-evolution of emission anisotropy is nonexponential. The outlined theory predicts that the total and magic-angle-detected fluorescence decays solely represent the kinetic fluorescence decay, and thereby, the emission anisotropy becomes an (multi)-exponential function of time for the excitation−detection cone half-angles not higher than about 15−20°. The initial values of the emission anisotropy are not modified by the application of the excitation−detection apertures if the cone half-angles do not exceed 10−15°. The histograms of unpolarized fluorescence, calculated from the parallel and the perpendicular components of polarized fluorescence, detected at the excitation−detection cones wider than about 65° solely represent the kinetic fluorescence decay. At such conditions, the microscope objective operates like an "integrating sphere". The calibration method, which is based on a general (symmetry adapted) formula describing fluorescence polarization experiments on macroscopically isotropic samples, is discussed. This method enables the analysis of all fluorescence polarization experiments without the necessity of considering the expressions for polarized fluorescence decays relating to a particular experimental case of interest. With this method, any commercially avaliable microscope objective can be calibrated, and its optical properties can be precisely verified. The application of the outlined theory to different fluorescence spectroscopy techniques is indicated. The expressions derived for confocal fluorescence polarization microscopy can be employed in the numerical analysis of the data recovered from the photochemical bioimaging.

1. Introduction

In many practical cases of different optical spectroscopy techniques (e.g., Raman and resonance Raman scattering,[1−8] one- or multiphoton-excitation fluorescence spectroscopy,[9−19] evanescent-wave-excitation fluorescence spectroscopy,[20−22] or fluorescence-detected linear dichroism[23]), high-aperture focusing and collecting lenses are used as the basic components of an experimental setup being employed in a given technique or, quite often, they are employed for obtaining the detected signals at proper signal-to-noise ratios. For example, in some experimental cases, the standard parallel-beam-excitation and/or -detection fluorescence measurements may lead to very weak fluorescence signals (e.g., for very thin molecular assemblies, for very low concentrations of the fluorophores, or in the case of fluorophores with extremely low quantum yield). This difficulty becomes particularly enhanced in the case of fluorescence spectroscopy with polarized light because the population density of excited-state molecules is drastically reduced due to photoselection of the ground-state molecules by linearly polarized exciting light, whereas the intensity of detected fluorescence is further reduced because the light is collected through an analyzer selecting a particular polarization of the fluorescence signal. In such cases, the intensity of fluorescence detected can be increased by performing the fluorescence polarization measurements under high-aperture-excitation and/or -detection experimental conditions. On the other hand, one- or multiphoton-excitation confocal fluorescence microscopy[10,16,23−25] and confocal (resonance) Raman microscopy[2−8] are the best examples of the optical spectroscopy techniques in which, by their nature, the objective lenses play the key role in the excitation and detection and in which the high-aperture-excitation and -detection experimental conditions are combined.

The high-aperture excitation and/or detection fluorescence polarization experiments require a modified theoretical description of the polarized fluorescence intensity, because the polarizations (directions of the electric field) of the exciting light and detected fluorescence are distributed within correspondingly wide cones at the focus, where the excitation and emission processes take place.

To our knowledge, the first treatment of the high-aperture-detection fluorescence polarization spectroscopy was presented

† To the memory of my dear daughter Karolina.

* E-mail: jjfisz@phys.uni.torun.pl.

10.1021/jp072113b CCC: $37.00
Published on Web 08/10/2007

by Dragsten.[13] He has derived the expressions describing the transformation of the Cartesian components of polarized fluorescence light emitted at the focus (focal space). The objective lens transforms the collected fluorescence into a parallel beam of light (laboratory space), which is then analyzed by a polarizer. By considering the so-called equivalent reflection planes, substituted for a lens, and by employing vector algebra, Dragsten has expressed the parallel ($I_{||}$) and perpendicular ($I_{\perp}$) components of polarized fluorescence, selected by an analyzer in the laboratory space, by two corresponding linear combinations of three Cartesian components of polarized fluorescence, emitted at the focus. Both linear combinations are expressed by the same set of three, normalized, transformation coefficients.[13]

Almost in parallel, the same problem was discussed by Axelrod.[14] To describe the high-aperture-detection fluorescence polarization, Axelrod has introduced a fantastic idea of employing the properties of the meridional planes,[26] which are defined by the optical axis of an objective lens and the rays propagating within the cone of the detected fluorescence. The expressions describing the relationships between the Cartesian components of polarized fluorescence in the focal and laboratory spaces, derived by Axelrod, are almost identical to the ones obtained by Dragsten,[13] which differ only in that the three transformation coefficients obtained by Axelrod are unnormalized. The high-aperture detection problem was further discussed by Axelrod in ref 27 for the case of fluorescence polarization microscopy, but without combining it with the high-aperture excitation case. In that paper, following the theory of electromagnetic field distribution in the region of focus by Richards and Wolf[26] that was further developed by Yoshida and Asakura[28] for the case of the coherent collimated Gaussian beams of light, Axelrod discussed the problem of the intensities of polarized components of the incident light at the focal plane, in particular, the dependence of these intensities on the ratio of the half-width of a Gaussian intensity profile and the focal length of an objective lens.

To our knowledge, the practical theory of fluorescence depolarization analysis for the microscopic measurements introduced by Koshioka, Sasaki, and Masuhara[11,12] was the first treatment to the problem of polarization effects in the confocal fluorescence microscopy in which the high-aperture-excitation and -detection conditions are combined. In this method, the microscopic polarized fluorescence decays $D_{||}$ and $D_{\perp}$, detected in the laboratory space through a depolarizer, are expressed in terms of the corresponding decays $I_{||}$ and $I_{\perp}$ that would be obtained from the traditional fluorescence polarization measurements, that is, $D_{||} \sim (1 - k_1)I_{||} + k_1 I_{\perp}$ and $D_{\perp} \sim k_2 I_{||} + (1 - k_2)I_{\perp}$, from which the decay of emission anisotropy $r(t) = (I_{||} - I_{\perp})/(I_{||} + 2I_{\perp})$ is reconstructed and analyzed. The parameters k_1 and k_2 are obtained from the microscopic measurements on a reference fluorophore that exhibits particular properties, namely, photophysics and rotational dynamics are monoexponential functions of time, and furthermore, the absorption and emission dipole moments are coaxial.

In our recent article[29] we have presented a derivation of the expressions describing high-aperture-excitation and/or -detection fluorescence spectroscopy with polarized light, involving the idea introduced by Axelrod,[14] using the meridional planes[26] to describe the transformation of polarization direction of the linearly polarized light passing through an objective lens. However, we have formulated this problem in the more convenient spherical coordinate representation, in which the excitation and emission processes are described in terms of the corresponding irreducible tensorial sets. This has allowed us to obtain a mathematical description of the combined high-aperture-excitation and -detection experimental conditions.

In this article we consider the problem of high-aperture-excitation and -detection fluorescence polarization spectroscopy for macroscopically isotropic molecular media (e.g., membrane suspensions and labeled macromolecules or solutions), for the case of one-photon excitations. We first discuss a derivation of the expression for polarized fluorescence decay in terms of irreducible tensorial sets (Section 2), and next, we recall the basic formulas that are well-known in traditional fluorescence polarization spectroscopy (i.e., the total fluorescence decay $I_{tot}(t)$, magic-angle-detected fluorescence decay $I_{mag}(t)$, unpolarized fluorescence decay $I_{unp}(t)$, and the emission anisotropy decay $r(t)$ at parallel-beam-excitation and -detection conditions; Section 3). In Section 4 we consider this problem again, but for the combined high-aperture-excitation and -detection experimental conditions. In particular, we display in more detail the effect of the laser beam cross-section intensity profile on the distribution of the fluorophores photoselected at the focus and on the fluorescence polarization detected.

In Section 5 we discuss the description of fluorescence polarization experiments for macroscopically isotropic molecular systems (e.g., membrane suspensions and labeled macromolecules or solutions) at high-aperture excitation and detection for a general geometric configuration (i.e., when the direction of excitation and direction of detection of polarized fluorescence make an arbitrary angle). We derive the expressions for parallel $I_{||}(t, \rho_0, \sigma_0, \Delta\psi)$ and perpendicular $I_{\perp}(t, \rho_0, \sigma_0, \Delta\psi)$ components of polarized fluorescence decays, where $\Delta\psi$ is the angle between the excitation and detection directions, and where ρ_0 and σ_0 are the excitation and detection cone half-angles. From these decays we obtain and then discuss the properties of the total fluorescence decay $I_{tot}(t, \rho_0, \sigma_0, \Delta\psi)$ and emission anisotropy decay $r(t, \rho_0, \sigma_0, \Delta\psi)$. A general conclusion that we draw is that at the high-aperture excitation or/and -detection conditions, $I_{tot}(t, \rho_0, \sigma_0, \Delta\psi)$ does not represent the decay of total fluorescence because the time evolution of $I_{tot}(t, \rho_0, \sigma_0, \Delta\psi)$ is not purely kinetic (i.e., there is a contribution from the dynamic evolution of photoselected fluorophores). This contribution depends on the excitation and detection cone half-angles, ρ_0 and σ_0, respectively. The emission anisotropy, at the same conditions, is a nonexponential function of time, and the manifestation of this property varies strongly with the change of ρ_0 and σ_0. The initial values of the emission anisotropy essentially depend on ρ_0 and σ_0.

By setting $\Delta\psi = 0°$ in all those expressions derived in Section 5, which concern the combined high-aperture-excitation and -detection, we immediately obtain the description of confocal fluorescence polarization microscopy (Section 6). This description is characterized by evident transparency and simplicity, and thereby, the content of Section 6 may find very serious practical applications in the analysis of time-resolved fluorescence lifetime imaging (FLIM), Förster resonance energy transfer (FRET), or in time-resolved emission anisotropy imaging. We examine, in a more systematic way, the basic properties of the total fluorescence decay $I_{tot}(t, \alpha_0)$, the emission anisotropy decay $r(t, \alpha_0)$, and the properties of both polarized fluorescence decays $I_{||}(t, \alpha_0)$ and $I_{\perp}(t, \alpha_0)$, where α_0 is the excitation−detection cone half-angle of a microscope objective. The term $I_{tot}(t, \alpha_0)$ does not solely represent the kinetic fluorescence decay because the decay of $I_{tot}(t, \alpha_0)$ is evidently contributed to by the dynamic evolution of photoselected fluorophores, in general experimental conditions. We show that $I_{tot}(t, \alpha_0)$ represents solely kinetic fluorescence decay at α_0 values lower than 15−20°. We also

demonstrate that the $r(t, \alpha_0)$ is a nonexponential function of time, in general experimental conditions. However, it becomes a multiexponential function of time for α_0 values lower than 15−20°, but a more accurate determination of the initial values of the emission anisotropy requires narrower excitation−detection cones (i.e., α_0 should not be higher than 10−15°). These predictions agree very well with the experimental conditions of typical confocal fluorescence microscopy studies, reported in the literature, aimed at the recovery of fluorescence lifetimes and emission anisotropy decay parameters (e.g., refs 16−19).

In the last part of Section 6 we derive the expressions for polarized fluorescence decays at combined high-aperture excitation and detection conditions, which relate to fluorescence polarization microscopy, for a coherent TEM_{00} exciting laser beam with a Gaussian intensity profile, with the application of the results of papers by Richards and Wolf,[26] by Yoshida and Asakura,[28] and by Axelrod.[27] The forms of the obtained expressions are identical with the corresponding ones derived with the application of the meridional plane properties.

By following the conception by Koshioka, Sasaki, and Masuhara[11] of using the reference fluorophore, in Section 7 we discuss the calibration method that enables one to analyze any one-photon-excitation fluorescence polarization experiment on an arbitrary, macroscopically isotropic sample. In this method, all fluorescence polarization experiments are described by one symmetry adapted formula, which is a linear combination of two time-dependent basis functions. The decay parameters describing the kinetic and dynamic evolution of excited-state fluorophores can be optimized without considering the explicit expressions that describe polarized fluorescence decays related to a particular experimental case of interest. Furthermore, this method enables one to experimentally compare and verify both descriptions of the fluorescence microscopy discussed in this article. Finally, with this method, any commercially avaliable microscope objective can be calibrated, and its optical properties can be precisely verified.

2. One-Photon-Excitation Polarized Fluorescence Decays

The intensity of polarized fluorescence decay can be described by the following relation (eq 1);[30]

$$I_{\hat{e}_i,\hat{e}_f}(t) = C\,\mathrm{Ph}(t) \int_{\Omega} \int_{\Omega_0} P_{ex}^{(\hat{e}_i)}(\Omega_0) f(\Omega_0) p(\Omega_0, 0|\Omega, t) P_{em}^{(\hat{e}_f)}(\Omega)\, d\Omega_0\, d\Omega \quad (1)$$

where C includes all constant factors and $\mathrm{Ph}(t)$ represents the kinetic fluorescence decay not coupled with rotational dynamics of fluorophores. $f(\Omega_0)$ describes the angular distribution of fluorophores, and in the case of a macroscopically isotropic system it equals $1/8\pi^2$. The term $p(\Omega_0, 0|\Omega, t)$ is the Green function describing the rotational dynamics of fluorophores. It describes a conditional probability for finding an excited molecule at time t and at angular orientation Ω, provided that it was excited at $t = 0$ and its orientation was Ω_0. The Euler angles $\Omega_0 = (\alpha_0, \beta_0, \gamma_0)$ and $\Omega = (\alpha, \beta, \gamma)$ describe the angular orientation of a molecule-fixed frame $X_M Y_M Z_M$ in the laboratory-fixed frame $X_L Y_L Z_L$, at time moments $t = 0$ and $t \geq 0$, respectively. The terms $P_{ex}^{(\hat{e}_i)}(\Omega_0)$ and $P_{em}^{(\hat{e}_f)}(\Omega)$ describe the angular dependence of the probabilities of excitation and detection of polarized fluorescence.[30]

$$P_{ex}^{(\hat{e}_i)}(\Omega) \sim |\mathbf{e}_i\, \hat{\mathbf{u}}_{ab}|^2 = (\hat{\mathbf{e}}_i \otimes \hat{\mathbf{e}}_i^*){:}(\hat{\mathbf{u}}_{ab} \otimes \hat{\mathbf{u}}^*_{ab}) = \mathbf{E}_i{:}\mathbf{A} \quad (2)$$

$$P_{em}^{(\hat{e}_f)}(\Omega) \sim |\mathbf{e}_f\, \hat{\mathbf{u}}_{em}|^2 = (\hat{\mathbf{e}}_f \otimes \hat{\mathbf{e}}_f^*){:}(\hat{\mathbf{u}}_{em} \otimes \hat{\mathbf{u}}^*_{em}) = \mathbf{E}_f{:}\mathbf{F} \quad (3)$$

The unit vectors (versors) $\hat{\mathbf{e}}_i$ and $\hat{\mathbf{e}}_f$ denote linear polarization of exciting and detected light, respectively, and versors $\hat{\mathbf{u}}_{ab}$ and $\hat{\mathbf{u}}_{em}$ denote the direction of absorption and emission dipole moments, respectively. Angular orientations of $\hat{\mathbf{e}}_i$, $\hat{\mathbf{e}}_f$, $\hat{\mathbf{u}}_{ab}$, and $\hat{\mathbf{u}}_{em}$ are described, in the $X_L Y_L Z_L$ frame, by polar angles $(\theta_i^{(L)}, \varphi_i^{(L)})$, $(\theta_f^{(L)}, \varphi_f^{(L)})$, $(\theta_a^{(L)}, \varphi_a^{(L)})$ and $(\theta_e^{(L)}, \varphi_e^{(L)})$, respectively. $\mathbf{E}_i = (\hat{\mathbf{e}}_i \otimes \hat{\mathbf{e}}_i)$, $\mathbf{E}_f = (\hat{\mathbf{e}}_f \otimes \hat{\mathbf{e}}_f)$, $\mathbf{A} = (\hat{\mathbf{u}}_{ab} \otimes \hat{\mathbf{u}}_{ab})$, and $\mathbf{F} = (\hat{\mathbf{u}}_{em} \otimes \hat{\mathbf{u}}_{em})$ are the second-rank Cartesian tensors defined as the tensor products of the corresponding vectors, where a tensor product of two vectors $\mathbf{a}$ and $\mathbf{b}$ is defined by $\mathbf{a} \otimes \mathbf{b} = [a_i b_j]$. The terms $\mathbf{E}_i$, $\mathbf{E}_f$, $\mathbf{A}$, and $\mathbf{F}$ are the excitation, detection, absorption, and emission tensors, respectively. The colon at the right-hand sides of eqs 2 and 3 means the scalar product of two Cartesian tensors, which for two second-rank Cartesian tensors, $\mathbf{A}$ and $\mathbf{B}$, is defined by the relation $\mathbf{A}{:}\mathbf{B} = \sum_{i,j} A_{ij} B_{ji}$. The relationship between the scalar products in Cartesian and spherical representations reads as shown in eq 4;

$$\mathbf{A}{:}\mathbf{B} = \sum_{K=0}^{2} A^{(K)} \odot B^{(K)} = \sum_{K=0}^{2} \sum_{m=-K}^{K} (-1)^m A_m^{(K)} B_{-m}^{(K)} \quad (4)$$

where $A^{(K)}$ and $B^{(K)}$ ($K = 0, 1, 2$) are two irreducible tensorial sets, and $A_m^{(K)}$ and $B_m^{(K)}$ ($m = -K, ..., K$) are their spherical components.[31,32]

Let versor $\hat{\mathbf{a}}$ represent one of the versors $\hat{\mathbf{e}}_i$, $\hat{\mathbf{e}}_f$, $\hat{\mathbf{u}}_{ab}$, or $\hat{\mathbf{u}}_{em}$. Then, the tensorial product $(\hat{\mathbf{a}} \otimes \hat{\mathbf{a}})$ can be expressed in terms of the corresponding product of spherical vector $a^{(1)}$, that is, in terms of irreducible tensorial sets $T^{(K)} = (a^{(1)} \otimes a^{(1)})^{(K)}$, where $K = 0, 1, 2$, and where [31,32]

$$T_m^{(K)} = (a^{(1)} \otimes a^{(1)})_m^{(K)} = \sum_{p,q=-1}^{1} C_{1,p}(\theta, \varphi) C_{1,q}(\theta, \varphi)\, C(11K; pq) \quad (5)$$

In this formula, the spherical components $a_p^{(1)}$ have been replaced by the modified spherical harmonics $C_{1,p}(\theta, \varphi) = \sqrt{4\pi/3}\, Y_{1,p}(\theta, \varphi)$, where (θ, φ) is the polar angles describing the orientation of $\hat{\mathbf{a}}$ in the laboratory frame, and $C(11K; pq)$ is the Clebsch−Gordan coefficients. Consequently, we obtain eq 6.

$$T_0^{(0)} = -\frac{1}{\sqrt{3}} \quad T_0^{(1)} = T_{\pm 1}^{(1)} = 0 \quad T_m^{(2)} = \sqrt{\frac{2}{3}} C_{2,m}(\theta, \varphi) \quad (m = 0, \pm 1, \pm 2) \quad (6)$$

The tensorial set $T^{(1)}$ disappears because $(\hat{\mathbf{a}} \otimes \hat{\mathbf{a}})$ is a symmetric Cartesian tensor. Finally, according to eq 4, $P_{ex}^{(\hat{e}_i)}(\Omega_0)$ and $P_{em}^{(\hat{e}_f)}(\Omega)$ take the forms shown in eqs 7 and 8.

$$P_{ex}^{(\hat{e}_i)}(\Omega_0) \sim E_i^{(0)} \odot A^{(0)} + E_i^{(2)} \odot A^{(2)} = \frac{1}{3} + \frac{2}{3} \sum_{m=-2}^{2} C_{2,m}^*(\theta_i^{(L)}, \varphi_i^{(L)}) C_{2,m}(\theta_a^{(L)}(0), \varphi_a^{(L)}(0)) \quad (7)$$

$$P_{em}^{(\hat{e}_f)}(\Omega) \sim E_f^{(0)} \odot F^{(0)} + E_f^{(2)} \odot F^{(2)} = \frac{1}{3} + \frac{2}{3}\sum_{m=-2}^{2} C_{2,n}(\theta_f^{(L)}, \varphi_f^{(L)}) C_{2,n}^*(\theta_e^{(L)}(t), \varphi_e^{(L)}(t)) \quad (8)$$

Taking into account the above results, the intensity of polarized fluorescence (eq 1) can be rewritten in the following form (eq 9).

$$I_{\hat{e}_i,\hat{e}_f}(t) = C\mathrm{Ph}(t)\langle P_{ex}^{(\hat{e}_i)}(\Omega_0) P_{em}^{(\hat{e}_f)}(\Omega)\rangle = C\mathrm{Ph}(t)(1 + 2\sum_{m=-2}^{2} C_{2,m}^*(\theta_i^{(L)}, \varphi_i^{(L)})\langle C_{2,m}(\theta_a^{(L)}(0), \varphi_a^{(L)}(0))\rangle + 2\sum_{m=-2}^{2} C_{2,n}(\theta_f^{(L)}, \varphi_f^{(L)})\langle C_{2,m}^*(\theta_e^{(L)}(t), \varphi_e^{(L)}(t))\rangle + 4\sum_{m,n=-2}^{2} C_{2,m}^*(\theta_i^{(L)}, \varphi_i^{(L)}) C_{2,n}(\theta_f^{(L)}, \varphi_f^{(L)}) \times \langle C_{2,m}(\theta_a^{(L)}(0), \varphi_a^{(L)}(0)) C_{2,n}^*(\theta_e^{(L)}(t), \varphi_e^{(L)}(t))\rangle \quad (9)$$

The second-rank modified spherical harmonics $C_{2,m}(\theta_i^{(L)}, \varphi_i^{(L)})$, $C_{2,n}(\theta_f^{(L)}, \varphi_f^{(L)})$, $C_{2,m}(\theta_a^{(L)}(0), \varphi_a^{(L)}(0))$, and $C_{2,n}(\theta_e^{(L)}(t), \varphi_e^{(L)}(t))$ represent the spherical components of tensors $\mathbf{E}_i$, $\mathbf{E}_f$, $\mathbf{A}$, and $\mathbf{F}$, respectively. The angular averages $\langle(...)\rangle$ denote the double integration occurring in eq 1.

Equation 9 concerns molecular systems of arbitrary macroscopic symmetry, that is, biaxial media (e.g., biaxial liquid crystals or some of the Langmuir−Blodgett (LB) films), uniaxial media (e.g., most of the LB films, planar membranes, or molecular monolayers deposited on a glass plate), membrane vesicles suspension, labeled macromolecules, and solutions. However, this formula can be adapted to a particular symmetry of the medium and to a particular symmetry of the fluorophores by projecting it into a symmetry adapted form with the application of appropriate projection operators.

For example, for media that are macroscopically isotropic (spherically symmetric), formula 9 must be totally symmetric with respect to an arbitrary rotation of the laboratory fixed-frame. In other words, this formula must be invariant with respect to all symmetry operations in a proper rotation group of symmetry $O^{(+)}$(eq 3). The symmetry adapted form of eq 9 is obtained by employing the projection operator shown in eq 10;

$$\hat{S}_{iso}[...] = \frac{1}{8\pi^2}\int_{\Omega'} R(\Omega')[...]\, d\Omega' \quad (10)$$

where $R(\Omega')$ is the rotation operator transforming the laboratory frame into a new orientation. Note that $R(\Omega')C_{2,m}(\theta^{(L)}, \varphi^{(L)}) = C_{2,m}(\theta^{(L)'}, \varphi^{(L)'})$, where $C_{2,m}(\theta^{(L)'}, \varphi^{(L)'})$ is the modified spherical harmonics in a new laboratory frame, and the relationship between both sets of modified spherical harmonics is given by $C_{2,m}(\theta^{(L)'},\varphi^{(L)'}) = \sum m' D_{mm'}^{(2)}(\Omega') C_{2,m'}(\theta^{(L)},\varphi^{(L)})$.[31,32] The application of eq 10 to a single modified spherical harmonics leads to eq 11

$$\hat{S}_{iso}[C_{2,n}(\theta^{(L)}, \varphi^{(L)})] = \sum_p (\int_{\Omega'} D_{np}^{(2)}(\Omega')\, d\Omega') C_{2,p}(\theta^{(L)}, \varphi^{(L)}) = 0 \quad (11)$$

because the integral takes the zero value.[31,32] This means that the second and third terms disappear in the symmetry adapted form of eq 9 because $\hat{S}_{iso}[C_{2,n}^*(\theta_i^{(L)},\varphi_i^{(L)})] = 0$ and $\hat{S}_{iso}[C_{2,n}(\theta_f^{(L)}, \varphi_f^{(L)})] = 0$, for each n and p. The application of eq 10 to the fourth term in eq 9 gives eq 12.

SCHEME 1

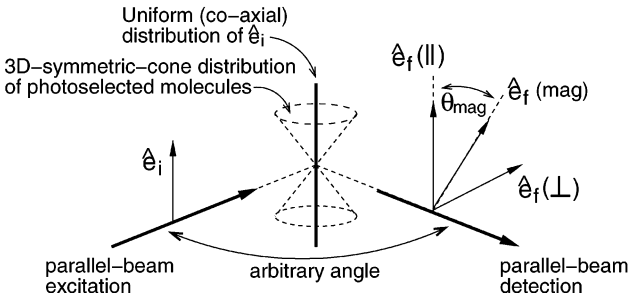

$$\hat{S}_{iso}[C_{2,m}^*(\theta_i^{(L)}, \varphi_i^{(L)}) C_{2,n}(\theta_f^{(L)}, \varphi_f^{(L)})] = C_{2,m}^*(\theta_i^{(L)'}, \varphi_i^{(L)'}) C_{2,n}(\theta_f^{(L)'}, \varphi_f^{(L)'}) = \sum_{p,q} (\int_{\Omega'} D_{mp}^{(2)*}(\Omega') D_{nq}^{(2)}(\Omega') d\Omega') C_{2,p}^*(\theta_i^{(L)}, \varphi_i^{(L)}) C_{2,q}(\theta_f^{(L)}, \varphi_f^{(L)}) = \frac{1}{5}\delta_{mn}\sum_p C_{2,p}^*(\theta_i^{(L)}, \varphi_i^{(L)}) C_{2,p}(\theta_f^{(L)},\varphi_f^{(L)}) \quad (12)$$

Finally, by replacing in eq 9 each product $C_{2,m}^*(\theta_i^{(L)},\varphi_i^{(L)}) C_{2,n}(\theta_f^{(L)},\varphi_f^{(L)})$ by the corresponding symmetry adapted linear combination (eq 12) and by neglecting the vanishing second and third term in eq 9, we obtain its symmetry adapted form (i.e., eq 13);

$$I_{\hat{e}_i,\hat{e}_f}(t) = C[\mathrm{Ph}(t) + 4/5(\sum_{p=-2}^{2} C_{2,p}^*(\theta_i^{(L)}, \varphi_i^{(L)}) C_{2,p}(\theta_f^{(L)}, \varphi_f^{(L)}))W(t)\mathrm{Ph}(t)] \quad (13)$$

where $W(t) = \sum_{m=-2}^{2} C_{2,m}^*(\theta_a^{(L)}(0),\varphi_a^{(L)}(0)) C_{2,m}^*(\theta_e^{(L)}(t),\varphi_e^{(L)}(t))\rangle$ is the symmetry adapted correlation function for rotational diffusion.

If the spherical components of the excitation and detection tensors do not require any further transformation, then the above formula can be replaced by the one commonly known in the literature (eq 14),[9]

$$I_{\hat{e}_i\hat{e}_f}(t) = C(\mathrm{Ph}(t) + 4/5P_2(\theta_{if}^{(L)})W(t)\mathrm{Ph}(t)) \quad (14)$$

where

$$P_2(\theta_{if}^{(L)}) = \sum_{p=-2}^{2} C_{2,p}^*(\theta_i^{(L)}, \varphi_i^{(L)}) C_{2,p}(\theta_f^{(L)}, \varphi_f^{(L)}) \quad (15)$$

and where $\theta_{if}^{(L)}$ is the angle between the versors $\hat{\mathbf{e}}_i$ and $\hat{\mathbf{e}}_f$ in the laboratory frame.

3. One-Photon Parallel-Beam-Excitation and -Detection Fluorescence Polarization Spectroscopy

In a traditional case of parallel-beam-excitation and -detection polarized fluorescence spectroscopy of marcoscopically isotropic samples (e.g., solutions, membrane vesicles suspension, or solution of labeled macromolecules), the fluorophores are excited by linearly polarized light (polarization versor $\hat{\mathbf{e}}_i$) and the emitted polarized fluorescence is detected at certain orientations of the analyzer (polarization versor $\hat{\mathbf{e}}_f$), as indicated in Scheme 1. The pulsed exciting light and the collected fluores-

cence both are parallel beams of light in the laboratory space and within the sample where the excitation and emission processes take place.

The photoselected molecules exhibit a three-dimensional (3D)-symmetric-cone-like angular distribution. The intensity of the detected polarized fluorescence is given by eq 14, and it does not depend on the angle between the directions of excitation and detection.

By setting the analyzer at $\theta_{if} = 0°$, $\theta_{if} = 90°$, and at the so-called magic angle $\theta_{if} = \theta_{mag} = 54.7°$, the expressions for the corresponding components of polarized fluorescence are given by the following equations according to eq 14.

$$I_{||}(t) = C(\mathrm{Ph}(t) + 4/5W(t)\mathrm{Ph}(t)) \quad (16)$$

$$I_{\perp}(t) = C(\mathrm{Ph}(t) - 2/5W(t)\mathrm{Ph}(t)) \quad (17)$$

$$I_{mag}(t) = C\mathrm{Ph}(t) \quad (18)$$

From the first two polarized fluorescence components the well-known expressions for the total fluorescence decay $I_{tot}(t)$, unpolarized fluorescence decay $I_{unp}(t)$, and emission anisotropy $r(t)$ decay can be evaluated, namely,

$$I_{tot}(t) = I_{||}(t) + 2I_{\perp}(t) = 3I_{mag}(t) \quad (19)$$

$$I_{unp}(t,) = I_{||}(t) + I_{\perp}(t) = C[\mathrm{Ph}(t) + 1/5W(t)\mathrm{Ph}(t)] \quad (20)$$

$$r(t) = \frac{I_{||}(t) - I_{\perp}(t)}{I_{tot}(t)} = 0.4W(t) \quad (21)$$

where C is a new constant factor.

Assuming that $\mathrm{Ph}(t)$ and $W(t)$ are multiexponential functions of time, that is, eq 22,

$$\mathrm{Ph}(t) = \sum_{i=1}^{N} a_i \exp(-t/\tau_{F,i}) \qquad W(t) = \sum_{j=1}^{M} b_j \exp(-t/\tau_{R,j}) \quad (22)$$

where

$$\sum_{i=1}^{N} a_i = 1 \text{ and } \sum_{j=1}^{M} b_i = P_2(\theta_{ae})$$

(where θ_{ae} is the angle between the absorption and emission dipole moments), eqs 19 and 21 become eqs 23 and 24, respectively;

$$r(t) = 0.4W(t) = 0.4\sum_{j=1}^{M} b_j \exp(-t/\tau_{R,j}) \quad (23)$$

$$I_{tot}(t) = 3I_{mag}(t) = 3C\sum_{i=1}^{N} a_i \exp(-t/\tau_{F,i}) \quad (24)$$

where a_i and $\tau_{F,i}$ are the kinetic fluorescence decay parameters, and b_j and $\tau_{R,j}$ are the emission anisotropy decay parameters. Consequently, $r(t)$ and $I_{tot}(t)$ are also multiexponential functions of time. It is important to stress here that these properties of the total (or magic-angle-detected) fluorescence and emission anisotropy decays play a fundamental role in a traditional fluorescence polarization spectroscopy with the parallel beam of exciting light and parallel beam of collected fluorescence. One has to remember, however, that in practice, except for unfocused laser excitation, these conditions are usually near-parallel rather than strictly parallel (i.e., the excitation and detection cones are narrow enough, at least within the medium containing the fluorophores, that for most practical purposes the convergence−divergence effects are negligible).

SCHEME 2

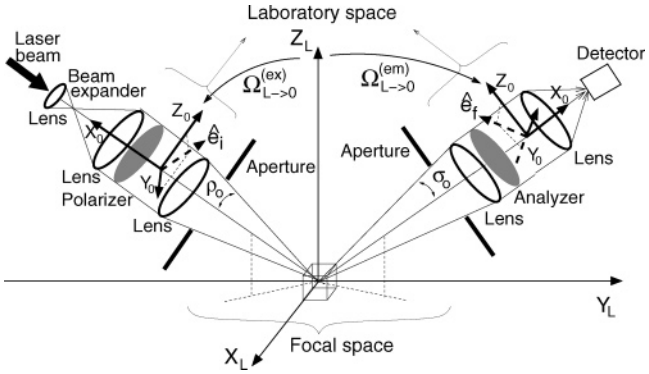

4. One-Photon-Excitation Fluorescence Polarization Spectroscopy at High-Aperture Excitation and Detection

In this section we consider a description of one-photon-excitation fluorescence polarization experiments under the high-aperture excitation and detection conditions, depicted in Scheme 2.

The pulsed parallel beam of exciting light passes through a beam expander. The polarizer selects the desired direction of polarization ($\hat{e}_i$) of the expanded exciting light that is then focused by a lens onto the sample. The fluorescence emitted from the sample is collected through an optical system composed of an aperture and a lens. The analyzer selects the desired direction of polarization ($\hat{e}_f$) of the parallel beam of fluorescence light that, afterward, is focused by a second lens onto the detector. Angular orientation of versors $\hat{e}_i$ and $\hat{e}_f$ in the laboratory frame $X_L Y_L Z_L$ are described by the polar angles ($\theta_i^{(L)}$, $\varphi_i^{(L)}$) and ($\theta_f^{(L)}$, $\varphi_f^{(L)}$). Both angular orientations can be expressed in terms of the polar angles of $\hat{e}_i$ and $\hat{e}_f$ in the coordinate frames $X_0 Y_0 Z_0$ in the excitation and detection channels (i.e., by ($\theta_i^{(0)}$, $\varphi_i^{(0)}$} and ($\theta_f^{(0)}$, $\varphi_f^{(0)}$)) and in terms of two sets of the Euler angles ($\Omega_{L\to 0}^{(ex)}$ and $\Omega_{L\to 0}^{(em)}$) defining the angular orientation of both $X_0 Y_0 Z_0$ frames with respect to the laboratory coordinate frame $X_L Y_L Z_L$.

In Scheme 2, the rays of the exciting beam of light, after passing through the polarizer, possess uniform polarization (i.e., all versors $\hat{e}_i$ are mutually parallel in the laboratory space). However, after being passed through a collecting lens (the rays are being transformed by this lens from the laboratory space to the focal space), versors $\hat{e}_i$ become appropriately distributed around the Z_0 axis at the focus, and the fluorophores are excited by the photons of different polarization directions. In other words, the photoselection does not proceed with one direction of polarization of the exciting light, in contrast to the parallel-beam-excitation condition, discussed in the previous section. The same concerns are present for the detection channel, where, in the focal space, the rays of the emitted fluorescence possess differently oriented versors $\hat{e}_f$, but after passing through the collecting lens (they are being transformed from the focal space to laboratory space) all rays become mutually parallel and all possess the same orientation of versors $\hat{e}_f$ selected by the analyzer. In other words, the uniform polarization $\hat{e}_f$ selected in the parallel beam of fluorescence light in the laboratory space

SCHEME 3

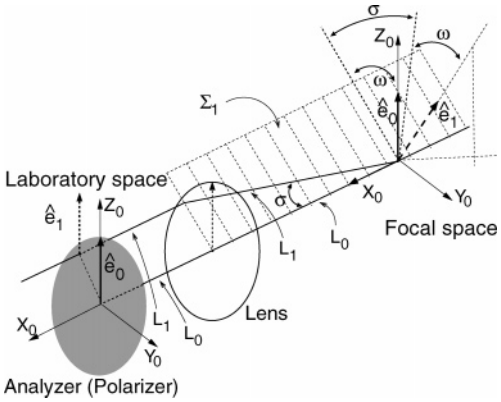

SCHEME 4

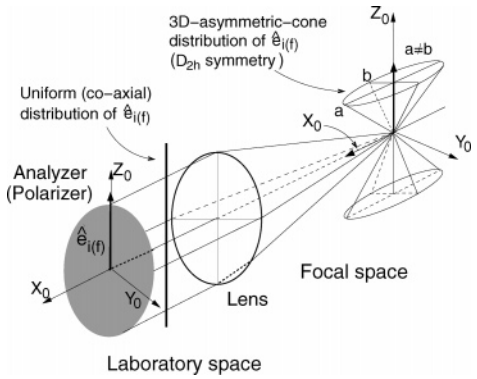

corresponds to a distribution of differently oriented versors $\hat{e}_f$ at the focus. Therefore, it is clear that the convergence−divergence effects discussed here must be taken into account when formulating a more accurate description of fluorescence polarization experiments at the conditions indicated in Scheme 2.

To better elucidate the problem in question, let us consider the situations depicted in Schemes 3 and 4, where parallel beams of exciting light or collected fluorescence, both uniformly polarized in the laboratory space, are transformed by a lens to/from the focal space, where the polarizations of both beams are given by the corresponding angular distributions.

According to Scheme 3, the ray of light L_0 propagating along the optical axis possesses the same polarization direction $\hat{e}_0$ in both spaces. This is in contrast to the ray L_1 because its polarization direction (versor $\hat{e}_1$) is differently oriented in both spaces. In the laboratory space L_1 is parallel to the optical axis, and $\hat{e}_1$ is parallel to $\hat{e}_0$ and to the Z_0 axis. In the focal space, L_1 makes an angle σ with the optical axis, and $\hat{e}_1$ makes an angle ω with the meridional plane Σ_1 (i.e., $\hat{e}_1$ is no longer parallel to the Z_0 axis at the focus).[26,14]

By considering several rays, one can figure out an approximate schematic visualization of the distributions of versors $\hat{e}_i$ and $\hat{e}_f$ at the focus, which correspond to the same versors parallelly oriented in the laboratory space. As shown in Scheme 4, in the focal space both distributions possess 3D-asymmetric-cone-like shapes of an elliptical cross-section (a D_{2h} symmetry), in contrast to uniform (coaxial) distributions of the same versors in the laboratory space.

It is clear, therefore, that $C_{2,p}(\theta_i^{(L)}, \varphi_i^{(L)})$ and $C_{2,p}(\theta_f^{(L)}, \varphi_f^{(L)})$ in eq 13 must be expressed in terms of the corresponding tensorial sets in the focal space, as we have discussed in ref 29, that is,

$$C_{2,p}(\theta_i^{(L)}, \varphi_i^{(L)}) = \sum_{q=-2}^{2} D_{pq}^{(2)*}(\Omega_{L\to 0}^{(ex)}) \sum_{s=-2}^{2} d_{qs}^{(2)}(-\pi/2) \times \sum_{r=-2}^{2} D_{sr}^{(2)*}(-\omega, -\sigma, \omega) C_{2,r}(\pi/2, \theta_i^{(0)}) \quad (25)$$

$$C_{2,p}(\theta_f^{(L)}, \varphi_f^{(L)}) = \sum_{q=-2}^{2} D_{pq}^{(2)*}(\Omega_{L\to 0}^{(em)}) \sum_{s=-2}^{2} d_{qs}^{(2)}(-\pi/2) \times \sum_{r=-2}^{2} D_{sr}^{(2)*}(-\omega', -\sigma, \omega') C_{2,r}(\pi/2, \theta_f^{(0)}) \quad (26)$$

where $D_{pq}^{(2)}(\Omega)$ and $d_{pq}^{(2)}(\beta)$ are the elements of Wigner and reduced Wigner rotational matrices,[31,32] respectively. The terms $\theta_i^{(0)}$ and $\theta_f^{(0)}$ are the angles between the versors $\hat{e}_i$ and $\hat{e}_f$ and the Z_0 axes of the $X_0Y_0Z_0$ coordinate frames in the excitation and detection channels in the laboratory space, as indicated in Scheme 2.

By employing the relationships in eqs 25 and 26, we obtain from eq 13 a formula for $I_{\hat{e}_i\hat{e}_f}(t, \rho, \omega, \sigma, \omega')$ describing the intensity of polarized fluorescence originating from a single-ray excitation and a single-ray detection. The fluorescence signal registered by the detector is the integrated intensity contributed to by all exciting and fluorescence rays propagating in the focal space within the cones of half angles ρ_0 and σ_0, correspondingly, that is,

$$I_{\hat{e}_i\hat{e}_f}(t, \rho_0, \sigma_0) = \int_0^{2\pi}\int_0^{\rho 0}\int_0^{2\pi}\int_0^{\sigma_0} I_{\hat{e}_i\hat{e}_f}(t, \rho, \omega, \sigma, \omega')\sin\rho\, d\rho\, d\omega \sin\sigma\, d\sigma\, d\omega' / \left(\int_0^{2\pi}\int_0^{\rho 0} \sin\rho\, d\rho\, d\omega \int_0^{2\pi}\int_0^{\sigma 0} \sin\sigma\, d\sigma\, d\omega'\right) \quad (27)$$

Finally, the formula describing the fluorescence intensity detected has the form of eq 13, with the spherical harmonics $C_{2,p}(\theta_i^{(L)}, \varphi_i^{(L)})$ and $C_{2,p}(\theta_f^{(L)}, \varphi_f^{(L)})$ given by eqs 28 and 29, respectively.[29]

$$C_{2,p}(\theta_i^{(L)}, \varphi_i^{(L)}) = \sum_{q=-2}^{2} D_{pq}^{(2)*}(\Omega_{L\to 0}^{(ex)}) \sum_{s=-2}^{2} R_s(\rho_0) d_{qs}^{(2)}(-\pi/2) C_{2,s}(\pi/2, \theta_i^{(0)}) \quad (28)$$

$$C_{2,p}(\theta_f^{(L)}, \varphi_f^{(L)}) = \sum_{q=-2}^{2} D_{pq}^{(2)*}(\Omega_{L\to 0}^{(em)}) \sum_{s=-2}^{2} Q_s(\sigma_0) d_{qs}^{(2)}(-\pi/2) C_{2,s}(\pi/2, \theta_f^{(0)}) \quad (29)$$

In the above expressions,

$$R_s(\rho_0) = \int_0^{\rho_0} d_{pp}^{(2)}(\rho)\sin\rho\, d\rho / \int_0^{\rho_0} \sin\rho\, d\rho \quad (30)$$

$$Q_s(\sigma_0) = \int_0^{\sigma_0} d_{pp}^{(2)}(\sigma)\sin\sigma\, d\sigma / \int_0^{\sigma_0} \sin\sigma\, d\sigma \quad (31)$$

where $s = 0, 1, 2$, and where $R_s(\rho_0)$ and $Q_s(\sigma_0)$ are the second-rank high-aperture excitation and detection transformation coefficients, respectively, in spherical representation. They transform the components of the second-rank excitation and detection spherical tensors between the laboratory and focal spaces, and

$$R_0(\rho_0) = 1/2(\cos\rho_0 - \cos^3\rho_0)/(1 - \cos\rho_0)$$

$$R_1(\rho_0) = 1/12(1 + 6\cos\rho_0 - 3\cos^2\rho_0 - 4\cos^3\rho_0)/(1 - \cos\rho_0)$$

$$R_2(\rho_0) = 1/12(7 - 3\cos\rho_0 - 3\cos^2\rho_0 - \cos^3\rho_0)/(1 - \cos\rho_0) \quad (32)$$

and

$$Q_0(\sigma_0) = 1/2(\cos\sigma_0 - \cos^3\sigma_0)/(1 - \cos\sigma_0)$$

$$Q_1(\sigma_0) = 1/12(1 + 6\cos\sigma_0 - 3\cos^2\sigma_0 - 4\cos^3\sigma_0)/(1 - \cos\sigma_0)$$

$$Q_2(\sigma_0) = 1/12(7 - 3\cos\sigma_0 - 3\cos^2\sigma_0 - \cos^3\sigma_0)/(1 - \cos\sigma_0) \quad (33)$$

where $R_s(\rho_0) = R_{-s}(\rho_0)$ and $Q_s(\sigma_0) = Q_{-s}(\sigma_0)$.

Note that the zero-rank transformation coefficients, $R_0^{(0)}(\rho_0)$ and $Q_0^{(0)}(\sigma_0)$, are proportional to the denominators in eqs 32 and 33, and their exact forms are $R_0^{(0)}(\rho_0) = 2\pi(1 - \cos\rho_0)$ and $Q_0^{(0)}(\sigma_0) = 2\pi(1 - \cos\sigma_0)$.

In the small-aperture limit for excitation (i.e., when $\rho_0 \rightarrow 0$) and detection (i.e., when $\sigma_0 \rightarrow 0$), we obtain eq 34,

$$\lim_{\rho_0\rightarrow 0} R_p(\rho_0) = 1 \quad \lim_{\sigma_0\rightarrow 0} Q_p(\sigma_0) = 1 \quad (p = 0, 1, 2) \quad (34)$$

and the relations given by eqs 27−29 automatically convert to the corresponding expressions discussed in the previous section for the parallel-beam excitation and detection experimental conditions. It is noteworthy that for the parallel-beam excitation and high-aperturedetection experimental conditions we get eq 35,

$$\lim_{\rho_0\rightarrow 0} R_p(\rho_0) = 1 \quad Q_p(\sigma_0) < 1 \quad (p = 0, 1, 2) \quad (35)$$

and for the opposed experimental case we get eq 36.

$$R_p(\rho_0) < 1 \quad \lim_{\sigma_0\rightarrow 0} Q_p(\sigma_0) = 1 \quad (p = 0, 1, 2) \quad (36)$$

The dependence of the transformation coefficients $R_p(\rho_0)$ and $Q_p(\sigma_0)$ on the cone half-angles ρ_0 and σ_0 is demonstrated in Figure 1a.

The transformation coefficients $R_p(\rho_0)$ given by eqs 30 and 32 refer to an expanded parallel beam of exciting light that possesses a homogeneous intensity in its cross-sections. However, in many experimental instances this assumption is not valid, and the single-mode continuous or pulsed laser beams of light exemplify such a situation. The light intensity inhomogeneity in the cross-section of a parallel beam of light is automatically converted by an objective lens into an inhomogeneous radial distribution of the light intensity in the converging beam, and this, of course, may essentially modify the angular distribution of fluorophores photoselected at the focus. A Gaussian profile of the intensity distribution of a TEM_{00} pulsed laser beam can be converted into a more homogeneous one, very close to a rectangular shape (the so-called flat-top or hat-top profiles). A typical beam-shaping telescope is the specially designed Galilean telescope,[33,34] which returns a collimated beam of light of homogeneous intensity distribution in its cross-section. Moreover, specially designed beam-shapers can also be applied to the high-power and short-pulse laser beams.

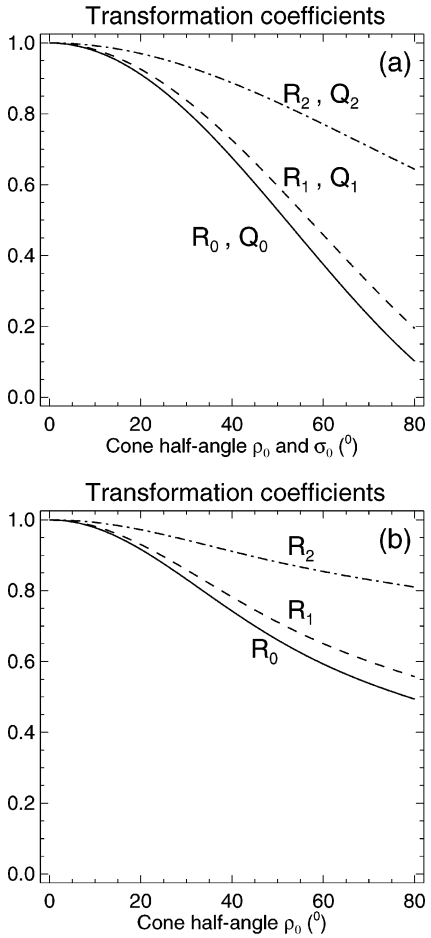

Figure 1. (a) Angular dependence of $R_p(\rho_0)$ and $Q_p(\sigma_0)$ for an uniform intensity distribution profile; (b) angular dependence of $R_p(\rho_0)$ for a Gaussian intensity profile (data obtained for $\Delta = 5$ mm and the focus length $f = 5$ mm).

On the other hand, however, the transformation coefficients $R_p(\rho_0)$, given by eq 32, can easily be modified to a Gaussian profile of the intensity of a (pulsed) laser beam. The Gaussian intensity profile $G(r)$ can be approximated by eq 37.

$$G(r) = A^2 \exp[-2r^2/\Delta^2] \quad (37)$$

Neglecting the aberration effect, the plane wavefront of a collimated laser beam is converted by an objective lens into a spherical wavefront, and hence, the sine condition $r = f \sin\rho$ holds, where f is the focal length. Consequently, the radial intensity distribution $G(\rho)$ in the focused beam can be approximated by eq 38,

$$G(\rho) = A^2 \exp[-2(f/\Delta)^2 \sin^2\rho] \quad (38)$$

where Δ is the half-width of the Gaussian profile. Finally, the modified definition of $R_p(\rho_0)$, previously given by eq 30, becomes eq 39.

$$R_p(\rho_0) = [\int_0^{\rho_0} G(\rho) d_{pp}^{(2)}(\rho) \sin\rho \, d\rho] / [\int_0^{\rho_0} G(\rho) \sin\rho \, d\rho] \quad (p = 0, 1, 2) \quad (39)$$

SCHEME 5

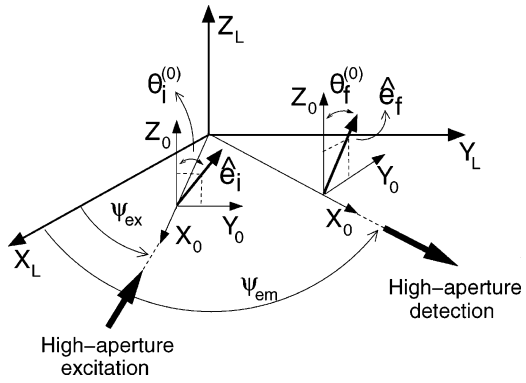

It is noteworthy that the amplitude (A) plays no role in eq 39. In Figure 1b we show the calculated transformation coefficients $R_p(\rho_0)$ for $\Delta = 5$ mm and for the focal length $f = 5$ mm. The results shown in Figure 1b demonstrate, quite clearly, that the nonuniform distribution of the intensity in the cross-section of a linearly polarized parallel beam of light, converted by an objective lens into the nonuniform radial distribution of the intensity in the focal space, may finally lead to a substantial modification of the angular distribution of photoselected molecules, as compared to the case when the intensity distribution profile is uniform (see Figure 1a).

5. Kinetic Fluorescence and Emission Anisotropy Decays at High-Aperture Excitation and Detection

Let us consider the fluorescence polarization experiments that can be performed according to the experimental arrangement depicted in Scheme 5. The beams of exciting and fluorescence light propagate in the X_LY_L plane of the laboratory frame $X_LY_LZ_L$ at angles ψ_{ex} and ψ_{em}. Desired polarizations of exciting light (angle $\theta_i^{(0)}$) and detected fluorescence (angle $\theta_f^{(0)}$) are selected in the $X_0Y_0Z_0$ frames in the excitation and detection channels, as shown in Scheme 5.

At these experimental conditions $\Omega_{L\to 0}^{(ex)} = (\psi_{ex}, 0, 0)$ and $\Omega_{L\to 0}^{(em)} = (\psi_{em}, 0, 0)$, and consequently, eqs 28 and 29 are replaced by eqs 40 and 41, respectively.

$$C_{2,p}(\theta_i^{(L)}, \varphi_i^{(L)}) = \sum_{s=-2}^{2} D_{ps}^{(2)*}(\psi_{ex}, -\pi/2, 0) R_s(\rho_0) C_{2,s}(\pi/2, \theta_i^{(0)}) \quad (40)$$

$$C_{2,p}^{*}(\theta_f^{(L)}, \varphi_f^{(L)}) = \sum_{s=-2}^{2} D_{ps}^{(2)}(\psi_{em}, -\pi/2, 0) Q_s(\sigma_0) C_{2,s}^{*}(\pi/2, \theta_f^{(0)}) \quad (41)$$

Consequently, the components $I_{||}(t, \rho_0, \sigma_0, \Delta\psi)$ (i.e., when $\theta_i^{(0)} = 0°$ and $\theta_f^{(0)} = 0°$) and $I_{\perp}(t, \rho_0, \sigma_0, \Delta\psi)$ (i.e., when $\theta_i^{(0)} = 0°$ and $\theta_f^{(0)} = 90°$), obtained from eq 13, take the forms shown in eqs 42 and 43, respectively,

$$I_{||}(t, \rho_0, \sigma_0, \Delta\psi) = C\{\mathrm{Ph}(t) + 1/20[6 \sin^2 \Delta\psi(R_0(\rho_0)Q_2(\sigma_0) + R_2(\rho_0)Q_0(\sigma_0)) + 3 \cos 2\Delta\psi(R_2(\rho_0)Q_2(\sigma_0) + R_0(\rho_0)Q_0(\sigma_0)) + 9R_2(\rho_0)Q_2(\sigma_0) + R_0(\rho_0)Q_0(\sigma_0)]W(t)\mathrm{Ph}(t)\} \quad (42)$$

$$I_{\perp}(t, \rho_0, \sigma_0, \Delta\psi) = C\{\mathrm{Ph}(t) - 1/20[6 \sin^2 \Delta\psi(R_0(\rho_0)Q_2(\sigma_0) - R_2(\rho_0)Q_0(\sigma_0)) + 3 \cos 2\Delta\psi(R_2(\rho_0)Q_2(\sigma_0) - R_0(\rho_0)Q_0(\sigma_0)) + 9R_2(\rho_0)Q_2(\sigma_0) - R_0(\rho_0)Q_0(\sigma_0)]W(t)\mathrm{Ph}(t)\} \quad (43)$$

where $\Delta\psi = \psi_{em} - \psi_{ex}$ is the angle between the direction of excitation and detection.

From the above expressions, we obtain eqs 44 and 45.

$$I_{tot}(t, \rho_0, \sigma_0, \Delta\psi) = I_{||}(t, \rho_0, \sigma_0, \Delta\psi) + 2I_{\perp}(t, \rho_0, \sigma_0, \Delta\psi) = C\{3\mathrm{Ph}(t) + 1/20[6 \sin^2 \Delta\psi(3R_2(\rho_0)Q_0(\sigma_0) - R_0(\rho_0)Q_2(\sigma_0)) + 3 \cos 2\Delta\psi(3R_0(\rho_0)Q_0(\sigma_0) - R_2(\rho_0)Q_2(\sigma_0)) - 9R_2(\rho_0)Q_2(\sigma_0) + 3R_0(\rho_0)Q_0(\sigma_0)]W(t)\mathrm{Ph}(t)\} \quad (44)$$

$$r(t, \rho_0, \sigma_0, \Delta\psi) = \frac{I_{||}(t, \rho_0, \sigma_0, \Delta\psi) - I_{\perp}(t, \rho_0, \sigma_0, \Delta\psi)}{I_{||}(t, \rho_0, \sigma_0, \Delta\psi) + 2I_{\perp}(t, \rho_0, \sigma_0, \Delta\psi)} = C\{1/10[6 \sin^2 \Delta\psi R_0(\rho_0)Q_2(\sigma_0) + 3 \cos 2\Delta\psi R_2(\rho_0)Q_2(\sigma_0) + 9R_2(\rho_0)Q_2(\sigma_0)]W(t)\mathrm{Ph}(t)\}/\{I_{tot}(t, \rho_0, \sigma_0) \quad (45)$$

For the parallel-beam excitation case $R_p(\rho_0) \to 1$, and eqs 42 and 43 are reduced to eqs 46 and 47, respectively.

$$I_{||}(t, \sigma_0) = C[\mathrm{Ph}(t) + 1/5(Q_0(\sigma_0) + 3Q_2(\sigma_0))W(t)\mathrm{Ph}(t)] \quad (46)$$

$$I_{\perp}(t, \sigma_0) = C[\mathrm{Ph}(t) - 1/5(-Q_0(\sigma_0) + 3Q_2(\sigma_0))W(t)\mathrm{Ph}(t)] \quad (47)$$

Consequently, the total fluorescence decay $I_{tot}(t, \sigma_0)$ and emission anisotropy decay $r(t, \sigma_0)$ become eqs 48 and 49, respectively.

$$I_{tot}(t, \sigma_0) = 3C[\mathrm{Ph}(t) + 1/5(Q_0(\sigma_0) - Q_2(\sigma_0))W(t)\mathrm{Ph}(t)] \quad (48)$$

$$r(t, \sigma_0) = 0.4\frac{Q_0(\sigma_0)W(t)}{1 + 1/5(Q_0(\sigma_0) - Q_2(\sigma_0))W(t)} \quad (49)$$

It is important to emphasize here that the last two relations do not depend on $\Delta\psi$. This is nothing surprising because, in this case, the fluorophores are excited by uniform (coaxial) distribution of versors $\hat{e}_i$ (i.e., all of these versors are parallel to the Z_L axis, and the angular distribution of excited molecules is cylindrically symmetric).

Additionally, for the parallel-beam detection case, $Q_p(\sigma_0) \to 1$, and the above four expressions further reduce to the ones given by eqs 16, 17, 19, and 21, according to what one might have expected.

The expressions derived in this section reflect a very particular character of fluorescence polarization spectroscopy at high-aperture-excitation and -detection experimental conditions, as compared to coresponding traditional expressions discussed in Section 2. The time evolution of polarized components in eqs 42 and 43 depends on the angle between the directions of excitation and detection of the fluorescence signal. This property is automatically reflected in the evolution of total fluorescence (eq 44) and emission anisotropy (eq 45) decays. Furthermore, the evolution of polarized fluorescence decays (eqs 42, 43, 46, and 47) are strongly dependent on the widths of the excitation and detection cones (i.e., the magnitude of the contribution of the kinetic−dynamic term $W(t)\mathrm{Ph}(t)$ to the evolution of these polarized fluorescence components depends very strongly on

the cone half-angles ρ_0 and σ_0). Consequently, the total fluorescence decays (eqs 44 and 48) do not solely represent the kinetic fluorescence decays because both decays are contributed to by the dynamic evolution of the photoselected fluorophores (i.e., by the rotational diffusion correlation function $W(t)$). This contribution is strongly modulated by the widths of the excitation and detection cones. This problem was encountered earlier by Axelrod[27] for a parallel-beam excitation and high-aperture detection experimental case, which is described by eqs 48 and 49.

In the case of the emission anisotropy, at the high-aperture excitation and detection conditions (see eq 45) or at parallel-beam excitation and high-aperture detection conditions (see eq 49), its time evolution is described by a nonexponential function of time because the denominators in eqs 45 and 49 contain the term proportional to $W(t)$. Moreover, the initial values of emission anisotropy ($r(t = 0, \sigma_0)$) are very strongly dependent on the values of the coefficients $R_p(\rho_0)$ and $Q_p(\sigma_0)$. It is clear, therefore, that the data obtained at both experimental conditions cannot be analyzed in terms of the emission anisotropy decay described by eq 23.

The case of parallel-beam excitation and high-aperture detection, discussed in this section (see eqs 48 and 49), is equivalent with the problems considered by Dragsten[13] and Axelrod,[14] and both described in the Cartesian coordinate representation. We want to demonstrate that the results of the treatments discussed in refs 13 and 14 are entirely equivalent with the results that can be obtained from our approach based on the spherical coordinate representation, introduced in ref 29 and further discussed in this article. Indeed, the components of polarized fluorescence $I_{||}(t, \sigma_0)$ and $I_{\perp}(t, \sigma_0)$ detected in the laboratory space, when related to the components of polarized fluorescence in the focal space, take the forms shown in eqs 50 and 51,

$$I_{||}(t, \sigma_0) = k'_a I_{\perp}^{(0)}(t) + k'_b I_{\perp}^{(0)}(t) + k'_c I_{||}^{(0)}(t) \quad (50)$$

$$I_{\perp}(t, \sigma_0) = k'_a I_{\perp}^{(0)}(t) + k'_c I_{\perp}^{(0)}(t) + k'_b I_{||}^{(0)}(t) \quad (51)$$

where $I_{||}^{(0)}(t)$ and $I_{\perp}^{(0)}(t)$ are the parallel and perpendicular components of fluorescence in the $X_0Y_0Z_0$ coordinate frame at the focus, and where the exciting beam of light is polarized along the Z_0 axis. The terms k'_a, k'_b, and k'_c are the normalized transformation coefficients obtained by Dragsten,[13] and they are equivalent with the coefficients obtained by Axelrod,[14] k_a, k_b, and k_c, after normalyzing them.[29] The normalized coefficients hold the closure property shown in eq 52,[29]

$$k'_a + k'_b + k'_c = 1 \quad (52)$$

which means that only two of these coefficients are necessary to describe the transformation between Cartesian components of polarized fluorescence from the focal space to laboratory space. Also, in the spherical representation only two transformation coefficients occur in all expressions derived (i.e., $R_0(\rho_0)$ and $R_2(\rho_0)$, see the final results obtained in previous sections). The coefficient $R_1(\rho_0)$, which is the odd moment of the second-rank spherical representation of the transformation in question, disappears due to the D_{2h} symmetry of the distribution of versors $\hat{\mathbf{e}}_f$ at the focus.

Polarized fluorescence components $I_{||}^{(0)}(t)$ and $I_{\perp}^{(0)}(t)$, in eqs 50 and 51, relate to the fluorescence components at the focus, and they are given by eqs 16 and 17, respectively. Therefore, eqs 50 and 51 can be rewritten as eqs 53 and 54, respectively.

$$I_{||}(t, \sigma_0) = C[\mathrm{Ph}(t) + 4/5(1/2(k'_c - k'_a) + 1/2(k'_c - k'_b))W(t)\mathrm{Ph}(t)] \quad (53)$$

$$I_{\perp}(t, \sigma_0) = C[\mathrm{Ph}(t) - 2/5((k'_a - k'_b) + (k'_c - k'_b))W(t)\mathrm{Ph}(t)] \quad (54)$$

Taking into account the following relationships between the transformation coefficients in both representations (eq 55)[29]

$$k'_c - k'_a = 1/2(Q_0(\sigma_0) + Q_2(\sigma_0))$$
$$k'_b - k'_a = 1/2(Q_0(\sigma_0) - Q_2(\sigma_0)) \quad (55)$$

and the closure property (eq 52), we immediately obtain from eqs 53 and 54 the coresponding formulas given by eqs 46 and 47.

6. Confocal Fluorescence Polarization Microscopy

The results obtained in previous sections can directly be adapted to the description of confocal fluorescence polarization microscopy. Let us assume that (as shown in Scheme 6) the pulsed-parallel beam of polarized laser light is reflected by a dichroic mirror and directed toward the objective and then it is focused on the sample. The term α_0 is the half-angle of the excitation and detection cone. The emitted fluorescence is collected by the same objective, and the parallel beam of fluorescence light passes (in the laboratory space) through an analyzer. By rotating the analyzer, a desired polarization of detected fluorescence can be selected (see the top view, as indicated in Scheme 6).

At the experimental conditions depicted in Scheme 6, $\Delta\psi = \psi_{em} - \psi_{ex} = 0$, $\rho_0 = \sigma_0 = \alpha_0$, and relations 42 and 43 lead to eqs 56 and 57, respectively,

$$I_{||}(t, \alpha_0) = C[\mathrm{Ph}(t) + 1/5(3R_2(\alpha_0)Q_2(\alpha_0) + R_0(\alpha_0)Q_0(\alpha_0))W(t)\mathrm{Ph}(t)] \quad (56)$$

$$I_{\perp}(t, \alpha_0) = C[\mathrm{Ph}(t) - 1/5(3R_2(\alpha_0)Q_2(\alpha_0) - R_0(\alpha_0)Q_0(\alpha_0))W(t)\mathrm{Ph}(t)] \quad (57)$$

where the distinguished direction in the laboratory space is the polarization of the exciting laser beam, which is parallel to the Z_0 axis of the $X_0Y_0Z_0$ coordinate frame.

Therefore, the total fluorescence $I_{tot}(t, \alpha_0)$ and emission anisotropy $r(t, \alpha_0)$ decays, obtained directly from eqs 44 and 45 or calculated from eqs 56 and 57, take the forms shown in eqs 58 and 59.

$$I_{tot}(t, \alpha_0) = 3C[\mathrm{Ph}(t) + 1/5(R_0(\alpha_0)Q_0(\alpha_0) - R_2(\alpha_0)Q_2(\alpha_0))W(t)\mathrm{Ph}(t)] \quad (58)$$

$$r(t, \alpha_0) = 0.4\frac{R_2(\alpha_0)Q_2(\alpha_0)W(t)}{1 + 1/5(R_0(\alpha_0)Q_0(\alpha_0) - R_2(\alpha_0)Q_2(\alpha_0))W(t)} \quad (59)$$

The detected intensity of polarized fluorescence decay at an arbitrary angle of polarization direction $\theta_f^{(0)}$ can be defined by eq 60.

$$I(t, \alpha_0, \theta_f^{(0)}) = \cos^2\theta_f^{(0)} I_{||}(t, \alpha_0) + \sin^2\theta_f^{(0)} I_{\perp}(t, \alpha_0) \quad (60)$$

However, an equivalent formula can be obtained directly from eq 13, with the spherical harmonics $C_{2,p}(\theta_i^{(L)}, \varphi_i^{(L)})$ and $C_{2,p}(\theta_f^{(L)}, \varphi_f^{(L)})$ adapted to the case depicted in Scheme 6. By

SCHEME 6

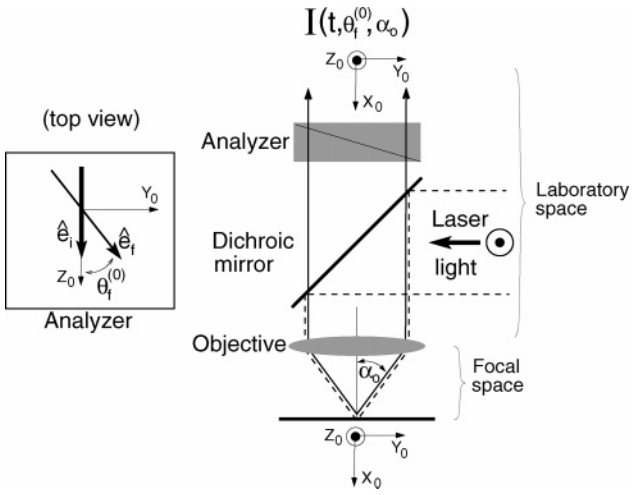

assuming, in eqs 25 and 26, that $(\theta_i^{(L)}, \varphi_i^{(L)}) = (0, \pi/2)$, $(\theta_f^{(L)}, \varphi_f^{(L)}) = (\theta_f^{(0)}, \pi/2)$, and $\Omega_{L\to 0}^{(ex)} = \Omega_{L\to 0}^{(em)} = (0, 0, 0)$, we obtain eqs 61 and 62,

$$C_{2,p}(\theta_i^{(L)}, \varphi_i^{(L)}) = \sum_{s=-2}^{2} d_{sp}^{(2)}(\pi/2) R_s(\rho_0) C_{2,s}(\pi/2, \theta_i^{(0)}) \quad (61)$$

$$C_{2,p}^{*}(\theta_f^{(L)}, \varphi_f^{(L)}) = \sum_{s=-2}^{2} d_{sp}^{(2)}(\pi/2) Q_s(\sigma_0) C_{2,p}^{*}(\pi/2, \theta_f^{(0)}) \quad (62)$$

and hence, finally, eq 13 becomes eq 63.

$$I(t, \alpha_0, \theta_f^{(0)}) = C[\mathrm{Ph}(t) + 1/5(R_0(\alpha_0)Q_0(\alpha_0) - R_2(\alpha_0)Q_2(\alpha_0) + 4P_2(\theta_f^{(0)})R_2(\alpha_0)Q_2(\alpha_0))W(t)\mathrm{Ph}(t)] \quad (63)$$

By setting the analyzer at $\theta_f^{(0)} = 0°$ and $\theta_f^{(0)} = 90°$, we obtain immediately from eqs 60 and 63 the expressions for polarized fluorescence components given by eqs 56 and 57, namely, $I(t, \alpha_0, 0°) \equiv I_{\parallel}(t, \alpha_0)$ and $I(t, \alpha_0, 90°) \equiv I_{\perp}(t, \alpha_0)$. Note that at the so-called magic angle ($\theta_f^{(0)} = 54.7°$), the term in eq 63 proportional to $P_2(\theta_f^{(0)})$, disappears because $P_2(54.7°) = 0$. It is important to note that the final form of eq 63 ($I_{mag}(t, \alpha_0)$) is contributed to by the kinetic−dynamic term $W(t)\mathrm{Ph}(t)$, which is in contrast to standard fluorescence spectroscopy (see eq 18).

If the intensity distribution in the cross-section of the exciting laser beam can be assumed as being homogeneous (e.g., it has been homogenized by a beam-shaping telescope), then the transformation coefficients of $R_p(\alpha_0)$ and $Q_p(\alpha_0)$ in the above relations are identical, and they are calculated according to eqs 32 or 33. However, if the intensity distribution is inhomogeneous and it can be approximated by a Gaussian profile, then thecoefficients of $R_p(\alpha_0)$ are calculated from eq 39, whereas $Q_p(\alpha_0)$ is evaluated from eq 33.

Equations 58 and 59 display the properties of fluorescence polarization experiments at high-aperture excitation and detection conditions, discussed in the previous section. The total fluorescence decay does not depend solely on the kinetic fluorescence decay $\mathrm{Ph}(t)$ because of the contribution of the second term proportional to the product $\mathrm{Ph}(t)W(t)$. The contribution of this term depends on the value of the cone half-angle (α_0). Emission anisotropy is a nonexponential function of time because the denominator in eq 59 contains the term proportional to$W(t)$. Furthermore, the initial value of emission anisotropy $r(t = 0, \alpha_0)$ very strongly depends on the value of α_0.

To justify the practical consequences of the above-mentioned properties of $I_{tot}(t, \alpha_0)$ and $r(t, \alpha_0)$, let us assume that $\mathrm{Ph}(t)$ and $W(t)$ are monoexponential functions of time with the fluorescence lifetime $\tau_F = 3$ ns and the rotational diffusion time $\tau_R = 0.7$ ns. The total fluorescence and emission anisotropy decays obtained from the measurements performed at the parallel-beam excitation and detection conditions will exhibit monoexponential time dependencies, with the corresponding decay times τ_F and τ_R, respectively. In the case of similar experiments at the combined high-aperture excitation and detection conditions the situation is different. The total fluorescence decay will be biexponential, with a long decay time $\tau_F = 3$ ns and a short decay time

$$\tau = \frac{\tau_F \tau_R}{\tau_F + \tau_R} \simeq 0.57 \text{ ns} \quad (64)$$

describing the decay time of the product function $W(t)\mathrm{Ph}(t)$, according to eq 58. Therefore, when analyzing such experimental data according to eq 24, one could come to an inappropriate conclusion that photophysical properties of fluorophores are described by two fluorescence lifetimes, $\tau_{F,1} = 3$ ns and $\tau_{F,2} = 0.57$ ns. In the case of emission anisotropy, the application of eq 23 would lead to a conclusion that the evolution of $r(t)$ is a bi- or triexponential. Furthermore, a value of $r(0)$ lower than 0.4 would be interpreted as resulting from the nonzero angle between the absorption and emission dipole moments.

In Figure 2a we show the plots of $I_{tot}(t, \alpha_0)$ calculated for $\mathrm{Ph}(t) = \exp(-t/\tau_F)$ and $W(t) = \exp(-t/\tau_R)$ with $\tau_F = 3$ ns and $\tau_R = 0.7$ ns, for $\alpha_0 = 0$, 20, 40 and 60°. The constant factor C in $I_{tot}(t, \alpha_0)$ was set to unity. The total fluorescence decay at $\alpha_0 = 0°$ is monoexponential, but for wider cone half-angles the decays become biexponential.

The changes of the contribution of the dynamical evolution of excited fluorophores to the detected intensity $I_{tot}(t, \alpha_0)$, with the change of α_0, can be well understood by considering the angular dependence of the coefficient $c_{tot}(\alpha_0)$,

$$c_{tot}(\alpha_0) = \frac{1}{5}(R_0(\alpha_0)Q_0(\alpha_0) - R_2(\alpha_0)Q_2(\alpha_0)) \quad (65)$$

which is the proportionality coefficient of the contribution of the kinetic−dynamic term $\mathrm{Ph}(t)W(t)$ in eq 58. According to Figure 2b, the absolute values of $c_{tot}(\alpha_0)$ rise very fast with the increasing values of α_0. At $\alpha_0 \simeq 62°$, the contribution of $\mathrm{Ph}(t)W(t)$ to $I_{tot}(t, \alpha_0)$ is the most pronounced, and its absolute contribution is about 9% (i.e., $|c_{tot}(62°)| \simeq 0.09$).

Taking into account the plot of $c_{tot}(\alpha_0)$ shown in Figure 2b, we may conclude that, for α_0 values not larger than about 15−20°, the total fluorescence decay (eq 58) can be reduced, to a very good approximation, to the first term (i.e., to $\mathrm{Ph}(t)$) because the contribution of the second term is less that 3% (i.e., the absolute values of $c_{tot}(\alpha_0)$ are lower than 0.03). At such conditions the experimentally detected decays of $I_{tot}(t, \alpha_0)$ can be analyzed according to eq 24. For wider excitation−detection cones, the participation of the kinetic−dynamic term $\mathrm{Ph}(t)W(t)$ in the time evolution of $I_{tot}(t, \alpha_0)$ cannot be assumed to be negligible, thereby taking into account only the values of $c_{tot}(\alpha_0)$. Also important is the mutual relation between the decay times τ_F and τ_R; three particular cases have to be distinguished, namely $\tau_R \gg \tau_F$, $\tau_R \simeq \tau_F$, and $\tau_R \ll \tau_F$. In the last case, the rotational dynamics is completed at the very beginning of the kinetic fluorescence decay, and hence, effectively, the fluores-

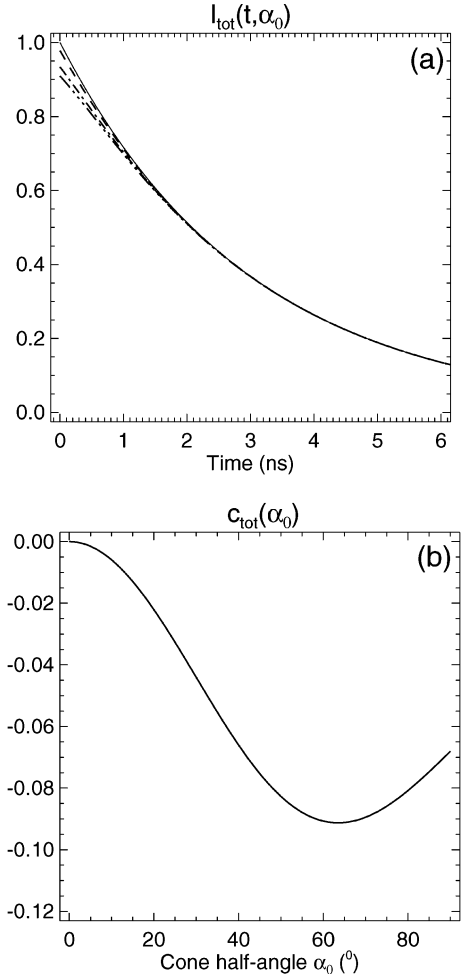

Figure 2. (a) Total fluorescence $I_{tot}(t)$ decays for $\alpha_0 = 0°$(—), $\alpha_0 = 20°$ (- - -), $\alpha_0 = 40°$ (- · - ·), and $\alpha_0 = 60°$ (- · · - · ·); (b) the contribution of the dynamic evolution of excited-state fluorophores to detected decays of the total fluorescence $I_{tot}(t, \alpha_0)$ as a function of α_0.

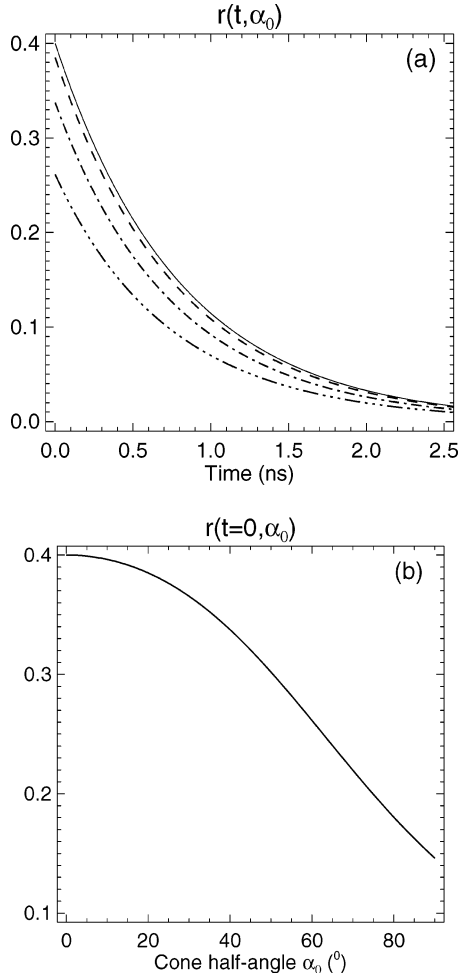

Figure 3. (a) Emission anisotropy $r(t, \alpha_0)$ decays for $\alpha_0 = 0°$ (—), $\alpha_0 = 20°$ (- - -), $\alpha_0 = 40°$ (- · - ·), and $\alpha_0 = 60°$ (- · · - · ·); (b) the dependence of initial values of emission anisotropy $r(t = 0, \alpha_0)$ on α_0. Results obtained for Ph(t) = exp(−t/3 ns) and$W(t)$ = exp(−t/0.7 ns).

cence signal detected at arbitrary angle α_0 will solely represent the kinetic decay of fluorescence.

In Figure 3a we show the calculated decays of the emission anisotropy $r(t, \alpha_0)$, which is a nonexponential function of time, and its initial values are strongly dependent on the values of α_0. For α_0 values lower than 15−20°, the decay of emission anisotropy becomes a multiexponential function of time because at such conditions the denominator in eq 59 does not contain the term proportional to $W(t)$ (i.e., $c_{tot}(\alpha_0)$ takes negligible values at such conditions, according to Figure 2b). However, the variation of the initial values of the emission anisotropy $r(t = 0, \alpha_0)$ on the change of α_0, calculated from eq 59 with the assumption that $W(t = 0) = 1$, that is, eq 66,

$$r(t = 0, \alpha_0) = 0.4\frac{R_2(\alpha_0)Q_2(\alpha_0)}{1 + 1/5(R_0(\alpha_0)Q_0(\alpha_0) - R_2(\alpha_0)Q_2(\alpha_0))} \quad (66)$$

shown in Figure 3b, indicates that a more precise recovery of the initial values of the emission anisotropy requires α_0 to be not higher than 10−15°.

It is worthy to consider the decays of parallel and perpendicular fluorescence components, given by eqs 56 and 57. The plots of $I_{||}(t, \alpha_0)$ and $I_{\perp}(t, \alpha_0)$ for $\alpha_0 = 0$, 20, 40, and 60°, obtained for Ph(t) = exp(−t/3 ns) and $W(t)$ = exp(−t/0.5 ns), are shown in Figures 4a and c. The angular dependences of the coefficients $c_{||}(\alpha_0)$ and $c_{\perp}(\alpha_0)$, which define the contribution of the product function Ph(t)$W(t)$ to both polarized components of fluorescence, that is, eqs 67 and 68,

$$c_{||}(\alpha_0) = 1/5(3R_2(\alpha_0)Q_2(\alpha_0) + R_0(\alpha_0)Q_0(\alpha_0)) \quad (67)$$

$$c_{\perp}(\alpha_0) = 1/5(3R_2(\alpha_0)Q_2(\alpha_0) - R_0(\alpha_0)Q_0(\alpha_0)) \quad (68)$$

are shown in Figures 4, panels b and d, respectively.

As is clearly shown in Figure 4 for the low aperture excitation−detection conditions (i.e., when α_0 does not exceed a value of 10−15°), both decays correspond to the ones given by eqs 16 and 17 because at such conditions $c_{||}(\alpha_0) \simeq 4/5$ and $c_{\perp}(\alpha_0) \simeq 2/5$. Note that this rigoristic limitation for the α_0 values is imposed mainly by the parallel component of fluorescence and by the coefficient $c_{||}(\alpha_0)$, in particular.

Very interesting is the case of the Y_0Z_0-plane-unpolarized fluorescence decay, defined in eq 69,

$$I_{unp}(t, \alpha_0) = I_{||}(t, \alpha_0) + I_{\perp}(t, \alpha_0) = C\left[\text{Ph}(t) + \frac{1}{5}R_0(\alpha_0)Q_0(\alpha_0)W(t)\text{Ph}(t)\right] \quad (69)$$

where C is a new constant factor. Also in this case, $I_{unp}(t, \alpha_0)$ contains a clear contribution of the dynamic evolution of photoselected fluorophores. For the paralle beam excitation and detection, the above formula becomes identical with eq 20. In

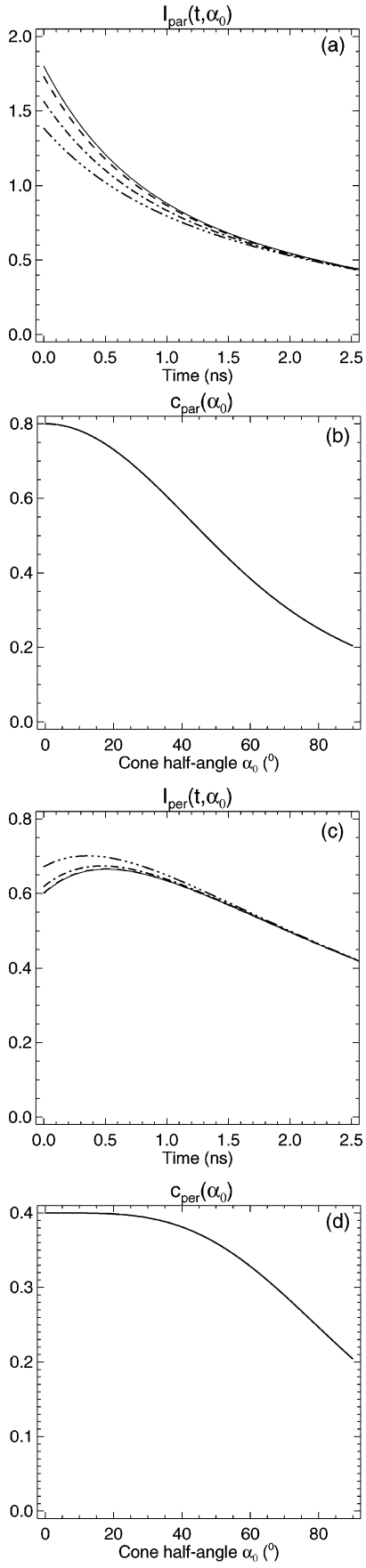

Figure 4. Angular dependence of (a) $I_{\parallel}(t, \alpha_0)$ and (c) $I_{\perp}(t, \alpha_0)$ for $\alpha_0 = 0°$ (—), $\alpha_0 = 20°$ (- - -), $\alpha_0 = 40°$ (- · - ·), and $\alpha_0 = 60°$ (- · · - · ·), with the assumption that $C = 1$; angular dependence of (b) $c_{\parallel}(\alpha_0)$ and (d) $c_{\perp}(\alpha_0)$.

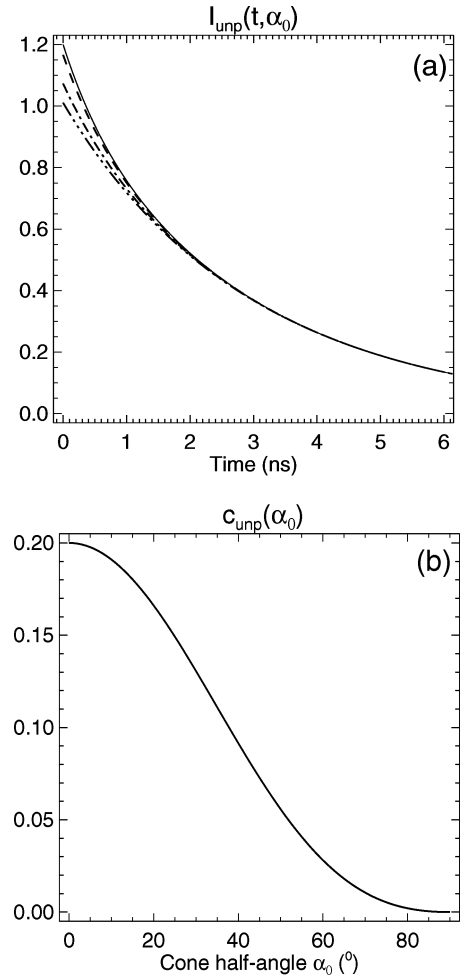

Figure 5. (a) The decays of $I_{unp}(t, \alpha_0)$ for $\alpha_0 = 0°$ (—), $\alpha_0 = 20°$ (- - -), $\alpha_0 = 45°$ (- · - ·), and $\alpha_0 = 70°$ (- · · - · ·), with the assumption that $C = 1$; (b) Angular dependence of $c_{unp}(\alpha_0)$.

Figure 5a we show the time-dependent plots of $I_{unp}(t, \alpha_0)$ for $\alpha_0 = 0$, 20, 45, and 70°, which demonstrate a clear modification of the time course of $I_{unp}(t, \alpha_0)$ with a change of the excitation−detection cone width. It is noteworthy that $I_{unp}(t, 70°)$ is identical with the $I_{tot}(t, 0°)$ shown in Figure 2a. Figure 5b displays the angular dependence of eq 70,

$$c_{unp}(\alpha_0) = \frac{1}{5} R_0(\alpha_0) Q_0(\alpha_0) \tag{70}$$

which is the proportionality coefficient of the contribution of the kinetic−dynamic term $\mathrm{Ph}(t)W(t)$ in eq 69.

A main conclusion that can be drawn from Figure 5b is that, for α_0 values greater than about 65°, the contribution of the term proportional to $\mathrm{Ph}(t)W(t)$ starts to be negligible because the values of $c_{unp}(\alpha_0)$ tend to zero at such wide excitation−detection cones. Hence, the unpolarized fluorescence decay calculated from two polarized decays $I_{\parallel,VHA}(t)$ and $I_{\perp,VHA}(t)$, detected separately at very high aperture (VHA), that is, eq 71,

$$I_{unp,VHA}(t) = I_{\parallel,VHA}(t) + GI_{\perp,VHA}(t) \sim \mathrm{Ph}(t) \tag{71}$$

represents, to a very good approximation, the kinetic fluorescence decay, solely. Therefore, $I_{unp,VHA}(t)$ has the same physical meaning as the total fluorescence decay ($I_{tot}(t)$) detected in the traditional fluorescence spectroscopy with parallel beams of exciting and detected light, and it can be analyzed according to eq 24. In other words, $I_{unp,VHA}(t)$ detected in the laboratory

space represents a fluorescence signal that can be understood as an integrated intensity over all angular orientations of the fluorophores emitting fluorescence at the focus, or equivalently, as an overall intensity given by $I_{X_0} + I_{Y_0} + I_{Z_0}$. At such conditions, the microscope objective behaves like an "integrating sphere".

The expressions for $I_{||}(t, \alpha_0)$ and $I_{\perp}(t, \alpha_0)$ can be derived by making use of the final results of the theory of electromagnetic field distribution in the region of focus by Richards and Wolf[26] and the results of the same theory developed by Yoshida and Asakura[28] for the case of the coherent collimated Gaussian beams of light focused by an objective lens. The Cartesian components of the electric field at the focal plane, along the three axes of the $X_0Y_0Z_0$ coordinate frame, are given by eqs 72−74,[26−28]

$$e_x(r, \phi, \alpha_0) \sim 2I_1(r) \cos \phi \tag{72}$$

$$e_y(r, \phi, \alpha_0) \sim -iI_2(r) \sin 2\phi \tag{73}$$

$$e_z(r, \phi, \alpha_0) \sim -i(I_0(r) + I_2(r) \cos 2\phi) \tag{74}$$

where the amplitude in common has been dropped, and where I_0-I_2 are defined by eqs 75−77.

$$I_0(r, \alpha_0) = \int_0^{\alpha_0} \sqrt{\cos \rho} \sin \rho (1 + \cos \rho) \exp(-(f/\Delta)^2 \sin^2 \rho) J_0(kr \sin \rho)\, d\rho \tag{75}$$

$$I_1(r, \alpha_0) = \int_0^{\alpha_0} \sqrt{\cos \rho} \sin^2 \phi \exp(-(f/\Delta)^2 \sin^2 \rho) J_1(kr \sin \rho)\, d\rho \tag{76}$$

$$I_2(r, \alpha_0) = \int_0^{\alpha_0} \sqrt{\cos \rho} \sin \phi (1 - \cos \rho) \exp(-(f/\Delta)^2 \sin^2 \rho) J_2(kr \sin \rho)\, d\rho \tag{77}$$

J_0, J_1, and J_2 are the Bessel functions of the first rank, and r and ϕ are the coordinates of any point in the focal plane. The term α_0 is the excitation−detection cone half-angle, and Δ is the half-width of the Gaussian intensity profile.

The fractional contribution of total intensity of the focused exciting light, polarized along the axes of the frame $X_0Y_0Z_0$ at the focus, can be defined as eqs 78−80.

$$f_x(\alpha_0) = |e'_x(\alpha_0)|^2 / \sum_{i=x,y,z} |e'_i(\alpha_0)|^2 \tag{78}$$

$$f_y(\alpha_0) = |e'_y(\alpha_0)|^2 / \sum_{i=x,y,z} |e'_i(\alpha_0)|^2 \tag{79}$$

$$f_z(\alpha_0) = |e'_z(\alpha_0)|^2 / \sum_{i=x,y,z} |e'_i(\alpha_0)|^2 \tag{80}$$

Hence, $f_x(\alpha_0) + f_y(\alpha_0) + f_z(\alpha_0) = 1$. The terms $e'_i(\alpha_0)$ ($i = x,y,z$) are the integrated values of $e_i(\alpha_0)$ over all r and ϕ. It is important to emphasize here that in the above formulas we have limited the integration solely to the focal plane. In more accurate considertions, this integration should be performed over all points of the region of focus that is the source of fluorescence detected through the pinhole. The intensities of polarized fluorescence emitted at the focus, and detected through a high aperture in the laboratory space, can be described as the corresponding linear combinations of the three fluorescence signals excited by the light polarized along the axes of the $X_0Y_0Z_0$ frame, namely, eqs 81 and 82,

$$I_{||}(t,\alpha_0) = f_x(\alpha_0) I_{x,||}(t, \alpha_0) + f_y(\alpha_0) I_{y,||}(t, \alpha_0) + f_z(\alpha_0) I_{z,||}(t, \alpha_0) \tag{81}$$

$$I_{\perp}(t, \alpha_0) = f_x(\alpha_0) I_{x,\perp}(t, \alpha_0) + f_y(\alpha_0) I_{y,\perp}(t, \alpha_0) + f_z(\alpha_0) I_{z,\perp}(t, \alpha_0) \tag{82}$$

where the constituent intensities $I_{i,||}(t, \alpha_0)$ and $I_{i,\perp}(t, \alpha_0)$ ($i = x,y,z$) can be obtained from eqs 42 and 43 with the assumption that $R_p(\alpha_0) \rightarrow 1$ and where

$$I_{x,||}(t, \alpha_0) = I_{x,\perp}(t, \alpha_0) = C[\mathrm{Ph}(t) - 2/5 Q_0(\alpha_0) W(t) \mathrm{Ph}(t)] \tag{83}$$

$$I_{y,||}(t, \alpha_0) = I_{z,\perp}(t, \alpha_0) = C[\mathrm{Ph}(t) - 1/5(-Q_0(\alpha_0) + 3Q_2(\alpha_0)) W(t) \mathrm{Ph}(t)] \tag{84}$$

$$I_{z,||}(t, \alpha_0) = I_{y,\perp}(t, \alpha_0) = C[\mathrm{Ph}(t) + 1/5(Q_0(\alpha_0) + 3Q_2(\alpha_0)) W(t) \mathrm{Ph}(t)] \tag{85}$$

Finally we obtain the following expressions (eqs 86 and 87),

$$I_{||}(t, \alpha_0) = C[\mathrm{Ph}(t) + 1/5(3A(\alpha_0) Q_2(\alpha_0) + B(\alpha_0) Q_0(\alpha_0)) W(t) \mathrm{Ph}(t)] \tag{86}$$

$$I_{\perp}(t, \alpha_0) = C[\mathrm{Ph}(t) - 1/5(3A(\alpha_0) Q_2(\alpha_0) - B(\alpha_0) Q_0(\alpha_0)) W(t) \mathrm{Ph}(t)] \tag{87}$$

where

$$A(\alpha_0) = f_z(\alpha_0) - f_y(\alpha_0),\ B(\alpha_0) = f_z(\alpha_0) + f_y(\alpha_0) - 2f_x(\alpha_0) \tag{88}$$

Note that $f_x(\alpha_0)$ can be replaced by $f_x(\alpha_0) = 1 - f_y(\alpha_0) - f_z(\alpha_0)$.

If the Gaussian intensity distribution of a (pulsed) laser beam is converted by a beam-shaping telescope into a rectangular profile and if the intensity distribution profile of exciting light, entering the microscope objective, can be assumed to be uniform, the term $\exp(-(f/\Delta)^2 \sin^2 \rho)$ in eqs 75−77 becomes replaced by unity.

The expressions derived for $I_{||}(t, \alpha_0)$ and $I_{\perp}(t, \alpha_0)$ exhibit exactly the same forms as the ones given by eqs 56 and 57. The only difference between both pairs of equations is that they differ in the high-aperture excitation coefficients, which are defined differently. Both pairs of equations can be written in an unified form, namely, eqs 89 and 90,

$$I_{||}(t, \alpha_0) = C[\mathrm{Ph}(t) + 1/5(3a(\alpha_0) + b(\alpha_0)) W(t) \mathrm{Ph}(t)] \tag{89}$$

$$I_{\perp}(t, \alpha_0) = C[\mathrm{Ph}(t) - 1/5(3a(\alpha_0) - b(\alpha_0)) W(t) \mathrm{Ph}(t)] \tag{90}$$

where $a(\alpha_0)$ and $b(\alpha_0)$ represent appropriate products of the high-aperture excitation and detection coefficients that occur in both descriptions of the confocal fluorescence microscopy. They can be calculated from the corresponding equations discussed in this article. They can also be determined experimentally by employing the calibration method, discussed in the next section.

7. Calibration Method

Equation 13 represents a general, symmetry adapted description of the time-resolved fluorescence polarization experiments on macroscopically isotropic samples (e.g., solutions, labeled macromolecules, and membrane vesicles) at arbitrary experi-

mental conditions (e.g., different adaptations of the arrangement depicted in Scheme 2). It can be rewritten in the following form (eq 91),

$$I(\{p\}, t) = C[\mathrm{Ph}(t) + KW(t)\mathrm{Ph}(t)] \quad (91)$$

where C and $K = 4/5\sum_{p=-2}^{2} C^{*}_{2,p}(\theta_i^{(L)},\varphi_i^{(L)})C_{2,p}(\theta_f^{(L)},\varphi_f^{(L)})$ are the constant factors at fixed experimental conditions, and $\{p\}$ is the set of all parameters defining the conditions of a particular experiment. For the experimental arrangement shown in Scheme 5, $\{p\} = \{\theta_i^{(0)}, \theta_f^{(0)}, \psi_{ex}, \psi_{em}, \rho_0, \sigma_0\}$, and in the case of a confocal microscope (Scheme 6), $\{p\} = \{\theta_f^{(0)}, \alpha_0\}$. Factor C depends on the intensity of the exciting light, on the intensities of absorption and emission bands at certain λ_{ex} and λ_{em}, and on the sensitivity of the detection channel to the detected polarization direction of fluorescence. The K term depends on the configuration of the experimental arrangement (e.g., on the polarization directions selected by the polarizer and analyzer), whereas it does not depend on the spectroscopic properties of the fluorophores. It is important to emphasize that all expressions for polarized fluorescence decays, derived in the previous sections, have the form of eq 91.

According to eq 91, $I(\{p\}, t)$ can be treated as the linear combination of the two time-dependend basis functions Ph(t) and $W(t)$Ph(t), namely eq 92,

$$I(\{p\}, t) = \gamma_1\mathrm{Ph}(t) + \gamma_2 W(t)\mathrm{Ph}(t) \quad (92)$$

where $\gamma_1 = C$ and $\gamma_2 = CK$ are the scalling factors, describing the degree of the contribution of both basis functions to $I(\{p\}, t)$ in a given experiment. Any linear combination of the intensities $I(\{p\}, t)$ has, finally, the form of eq 92. Hence, the effects of the experimental artifacts (e.g., reflection of the fluorescence light at the objective lens or aberration effects) will be accumulated in the scaling factors, and they are compensated for by the calibration method discussed below.

Equations 91 and 92 contain two sets of unknown parameters (i.e., two constants) and the decay parameters of Ph(t) and $W(t)$. If one of these two sets of parameters is known, the second one can be recovered from the data analysis. Because eq 92 contains two time-dependent basis functions, at least two polarized fluorescence decays, with possibly most different contributions of both basis functions, must be collected and subjected to simultaneous (global) analysis.

Let us assume that the decay parameters of $Ph_c(t)$ and $W_c(t)$ (see eq 22), for an arbitrary fluorophore in a solution phase, have been determined from the standard time-resolved fluorescence polarization experiment. Hence, the δ-pulse-excitation forms of $Ph_c(t)$ and $W_c(t)$ are known. Next, we collect two distinct polarized fluorescence decays for the same sample on the experimental arrangement (an instrument) that we want to calibrate. It does not matter whether we consider the experimental arrangement depicted in Schemes 5 or 6 or if we consider a much more complicated one. It also does not matter which of the angles (i.e., $\theta_i^{(0)}$, $\theta_f^{(0)}$, ψ_{ex}, or ψ_{em}) has been modified when changing the experimental conditions in Scheme 5 in order to collect the second (distinct) decay. The two detected, distinct polarized fluorescence decays are described by eqs 93 and 94.

$$I_c(\{p\}_1, t) = \gamma_{c,1}\mathrm{Ph}_r(t) + \gamma_{c,2}W_c(t)\mathrm{Ph}_c(t) \quad (93)$$

$$I_c(\{p\}_2, t) = \gamma'_{c,1}\mathrm{Ph}_c(t) + \gamma'_{c,2}W_c(t)\mathrm{Ph}_c(t) \quad (94)$$

Because the δ-pulse-excitation forms of $Ph_c(t)$ and $W_c(t)$ are known, two pairs of scalling parameters ($\gamma_{c,1}$, $\gamma_{c,2}$ and $\gamma'_{c,1}$, $\gamma'_{c,2}$) can be recovered by means of a multiple linear regression method applied independently to each of the above equations. Hence, the values of the constant factors $C_{c,1}$, $K_{c,1}$ and $C_{c,2}$, $K_{c,2}$ can be calculated. The recovered values of $K_{c,1}$ and $K_{c,2}$ can be treated as the calibration parameters in the analysis of two polarized fluorescence decays detected at the same experimental conditions as in the former case, for another sample with the same or another fluorophore, that is, eqs 95 and 96,

$$I_s(\{p\}_1, t) = C_{s,1}[\mathrm{Ph}(t) + K_{c,1}W(t)\mathrm{Ph}(t)] \quad (95)$$

$$I_s(\{p\}_2, t) = C_{s,2}[\mathrm{Ph}(t) + K_{c,2}W(t)\mathrm{Ph}(t)] \quad (96)$$

where the decay parameters of Ph(t) and $W(t)$ and the constant factors $C_{s,1}$ and $C_{s,2}$ have to be recovered from the global analysis of the data.

If the excitation conditions in both measurements of polarized fluorescence decays, for both sample, are identical and if the experimental conditions have been changed (to collect two distinct decays) by setting another orientation of the analyzer, then the number of fitted parameters in the analysis of the data obtained for the sample studied can be reduced. Indeed, in such cases $C_{c,1}$ and $C_{c,2}$ differ solely by different sensitivity of the detection channel on the polarization direction of fluorescence detected (the so-called G-factor problem; i.e., $G = C_{c,2}/C_{c,1}$). Consequently, $C_{s,2}$ in eq 96 becomes replaced by $GC_{s,1}$; hence, one constant factor has been eliminated from the list of the fitted parameters. Finally, the total number of parameters to be fitted in eqs 95 and 96 is the same as in the standard fluorescence polarization experiments.

The calibration method discussed here is general, and it applies to all one-photon-excitation fluorescence polarization experiments on macroscopically isotropic samples. A fundamental advantage of this method is that it eliminates the necessity of derivation of the explicit expressions for polarized fluorescence decays, corresponding to a particular experimental case of interest. In the case of confocal fluorescence microscopy, the comparison of eqs 89 and 90 with eqs 95 and 96 leads to the following relationships (eq 97),

$$a(\alpha_0) = \frac{5}{6}(K_{c,1} - K_{c,2}) \quad b(\alpha_0) = \frac{5}{2}(K_{c,1} + K_{c,2}) \quad (97)$$

which enable one to experimentally compare and verify both descriptions of the fluorescence microscopy discussed in this article. Futhermore, for the parallel-beam excitation and high-aperture detection experimental conditions, $a(\alpha_0) = 3Q_2(\alpha_0)$ and $b(\alpha_0) = Q_0(\alpha_0)$; hence, the calibration method enables one to verify the optical properties of any microscope objective. Note that the expressions for $Q_0(\alpha_0)$ and $Q_2(\alpha_0)$ have been derived for an ideal objective lens, for which such effects as the reflection of fluorescence light and chromatic and spherical aberration do not occur.

8. Discussion

The theory outlined in this article may find interesting applications in many problems important from the experimental point of view. Equations 42−45 (Section 5), simplified to the perpendicular excitation−detection experimental configuration (i.e., when $\Delta\psi = 90°$), can be applied in the analysis of high-aperture-excitation and/or -detection fluorescence polarization studies of the membrane vesicles suspensions, which are treated as the models of biological membranes. The objective lenses

increase the fluorescence signal detected, and this allows one to essentially reduce the concentration of the fluorophores embedded in the membranes, which has an evident advantage because the experiments at very low concentrations of the fluorophores are definitely less invasive. The same pertains to labeled proteins incorporated into the membranes. Furthermore, the same formulas, after appropriate adaptation, can be used in the analysis of the excited-state processes of the fluorophores embedded in a membrane suspension or in a solution phase, in particular, when the fluorescence signals emitted by the photoproducts are very low.

Equations 46−49, describing the parallel-beam-excitation and high-aperture-detection fluorescence polarization experiments, can be used in the description of the evanescent-wave-excitation fluorescence polarization experiments on isotropically distributed fluorophores at different kinds of interfaces. These relations apply to the standard, one-excited-state problem, but they can be easily adapted to the cases when the fluorophores undergo different kinds of excited-state processes at the interfaces.

The expressions obtained in Section 6, which describe confocal fluorescence polarization microscopy, enable very precise identification of the relaxation times associated with the kinetic fluorescence decay and those associated with the dynamic evolution of the photoselected fluorophores. Hence, the expressions obtained in Section 6 may find a successful applications in the confocal fluorescence microscopy studies of microscopic photochemical (microphotochemical) properties of the compounds undergoing intramolecular charge transfer (ICT), twisted intramolecular charge transfer (TICT), and intramolecular proton transfer (IPT) processes in different media, including the interfaces. On the other hand, because of the high sensitivity of ICT, TICT, and IPT processes to environmental properties (e.g., local polarity, polarizability, local viscosity, and all other physicochemical local properties of the medium), the fluorophores exhibiting such properties can be used as the probe molecules in the photochemical bioimaging on a pixel-by-pixel basis, leading to a deeper insight into the properties of a biomedical sample under study. In such studies, to each pixel an experimentally detected multiexponential fluorescence decay surface can be ascribed, which can be subjected to numerical optimization aimed at the recovery of the fluorescence decay times and the corresponding emission- or excitation-wavelength-dependent set of the amplitudes (pre-exponential factors). Such analyses can be radically accelerated by the application of an optimizer that separates the linear (e.g., the amplitudes) from the nonlinear (e.g., the fluorescence decay time) model parameters, where the linear parameters are being recovered from the multiple linear regresion. Such properties possess the variable projection (VP) optimization method and its numerical implementation VAPRO[35,36] and CORE optimizer.[37] The optimizer based on the convolved autoregressive model is very important.[38] It is a specially designed method for the analysis of the fluorescence microscopy data. In our recent article[39] we introduced a genetic-algorithm-based optimization method (GA-MLR) that combines genetic algorithm (GA) and multiple linear regression (MLR) methods, where nonlinear parameters are fitted by GA and the linear parameters are calculated from MLR. As was demonstrated in ref 39, a combination of the GA-MLR optimization method with the algorithm outlined in ref 40, designed for the analysis of fluorescence decays of the compounds undergoing the ICT, TICT, and IPT processes, may be a very suitable optimization method in the analysis of the data obtained from the photochemical bioimaging (e.g., the recovery of the images of fluorescence lifetimes of both excited states, the images of individual kinetic rates involved in the excited-state relaxation process and the images of the amplitudes and relative shifts of the emission bands of both excited-state species).

Acknowledgment. I would like to give thanks to Paul Dragsten for sending me the copy of the Appendix of his Ph.D. thesis and for discussions, to Professor Hiroshi Masuhara for sending me the copies of the papers cited in this article, to Alexander Laskin (MolTech GmbH, Berlin) for the valuable discussion about the properties and applications of the beam-shapers, and to Professor Peter Stilbs for informing me about the CORE optimizer. I would also like to thank both referees for helpful comments.

References and Notes

(1) Carey, P. R. *Biochemical Application of Raman and Resonance Raman Spectroscopies*; Academic Press: Paris, San Diego, San Francisco, Sao Paulo, Sydney, Tokyo, Toronto, 1982.
(2) Barry, B.; Mathies, R. A. *J. Cell Biol.* **1982**, *94*, 479−482.
(3) Barry, B.; Mathies, R. A. *Biochemistry* **1987**, *26*, 59−64.
(4) Clark, R. J. H. *Chem. Soc. Rev.* **1995**, *24*, 187−196.
(5) Goulet, P.; Pieczonka, Acoca, N., R. F. *Microsc. Microanal.* **2003**, *9*, 1080−1081.
(6) Cheng, J. X.; Xie, X. S. *J. Phys. Chem. B.* **2004**, *108*, 827−840.
(7) Baena, J. R.; Lendl, B.; *Curr. Opin. Chem. Biol.* **2004**, *8*, 534−539.
(8) Bierlinger, N.; Schwanninger, M. *Plant Physiol.* **2006**, *140*, 1246−1254.
(9) Lakowicz, J. R. *Principles of Fluorescence Spectroscopy*; Kluwer Academic/Plenum Publishers: New York, Boston, Dordrecht, London, Moscow, 1999.
(10) Denk, W.; Strickler, J. H.; Webb, W. W. *Science* **1990**, *248*, 73−76.
(11) *Microchemistry*; Masuhara, H., Ed.; Elsevier: Amsterdam, 1994.
(12) Koshioka, M.; Sasaki, K.; Masuhara, H., *Appl. Spectrosc.* **1995**, *49*, 224−228.
(13) Dragsten, P. R. *Mechanism of Voltage-Induced Fluorescence Changes of the Membrane Probe Merocyanine 540. A Fluorescence Polarization Study*; Ph.D. thesis, Cornell University: United States of America, 1977.
(14) Axelrod, D. *Biophys. J.* **1979**, *26*, 557−574.
(15) Gerritsen, H. C.; Grauw, C. J. *One and Two-Photon Confocal Fluorescence Lifetime Imaging and its Applications*; Oxford University Press; Oxford, 2001.
(16) Vishwasrao, H. D.; Heikal, A. A.; Kasischke, K. A.; Webb, W. W. *J. Biol. Chem.* **2005**, *280*, 25199−25126.
(17) Bigelow, C. E.; Harkrider, C. J.; Conover, D. L.; Foster, T. H.; Georgakoudi, I.; Mitra, S.; Nichols, M. G.; Rajadhyaksha *Rev. Sci. Instrum.* **2001**, *72*, 3407−3410.
(18) Bigelow, C. E.; Conover, D. L.; Foster, T. H. *Opt. Lett.* **2003**, *28*, 695−697.
(19) Bigelow, C. E.; Vishwasrao, H. D.; Frelinger, J. G.; Foster, T. H. *J. Microsc.* **2004**, *215*, 24−33.
(20) Axelrod, D. *J. Cell Biol.* **1981**, *89*, 141−145.
(21) Burmeister, J. S.; Truskey, G. A.; Reichert, W. M. *J. Microsc.* **1994**, *173*, 39−51.
(22) Stock, K.; Sailer, R.; Strauss, W. S. L.; Lyttek, M.; Steiner, R.; Schneckenburger, H. *J. Microsc.* **2003**, *211*, 19−29.
(23) Benninger, R. K. P.; Önfelt, B.; Neil, M. A. A.; Davis, M. D.; French, P. M. W. *Biophys. J.* **2005**, *88*, 609−622.
(24) König, K. *J. Microsc.* **2000**, *200*, 83−86.
(25) Pawley, J. B. *Handbook of Biological Confocal Microscopy*; Plenum Press - Springer: New York, 2006.
(26) Richards, B.; Wolf, E. *Proc. R. Soc. Lond. A. Math. Phys. Sci.* **1959**, *253*, 358−379.
(27) Axelrod, D. *Methods Cell Biol.* **1989**, *30*, 333−352.
(28) Yoshida, A.; Asakura, T. *Optik* **1974**, *41*, 281−292.
(29) Fisz, J. J.; Buczkowski, M.; Zuchowski, P. *Chem. Phys. Lett.* **2005**, *412*, 263−268.
(30) Fisz, J. J. *Chem. Phys.* **1985**, *99*, 177−191.
(31) Rose, M. E. *Elementary Theory of Angular Momentum*; Wiley: New York, 1957.
(32) Brink, D. M.; Satchler, G. R. *Angular Momentum*; Oxford University Press:Oxford, 1968.
(33) Hoffnagle, J. A.; Jefferson, C. M. *Appl. Opt.* **2000**, *39*, 5488−5499.

(34) Dickey, F. M.; Holswade, S. C. *Laser Beam Shaping, Theory and Techniques*; Marcel Dekker, New York, 2000.
(35) Golub, G. H.; Pereyra, V. *SIAM J. Numer. Anal.* **1973**, *10*, 413−432.
(36) Golub, G.; Pereyra, V. *Inverse Probl. Eng.* **2003**, *19*, R1−R26.
(37) Stilbs, P.; Palusen, K. *Rev. Sci. Instrum.* **1996**, *67*, 4380−4386.
(38) Sasaki, K.; Masuhara, H., *Appl. Opt.* **1991**, *30*, 997.
(39) Fisz, J. J. *J. Phys. Chem. A.* **2006**, *110*, 12977−12985.
(40) Fisz, J. J. *Chem. Phys.* **1995**, *192*, 163−188.